Alignment and Patterning of Ordered Small-molecule Organic Semiconductor Micro/nanocrystals for Device Applications

DOI: 10.1002/ ((please add manuscript number))
Article type: Review

Alignment and Patterning of Ordered Small-molecule Organic Semiconductor Micro/nanocrystals for Device Applications

Xiujuan Zhang, Jiansheng Jie, Wei Deng, Qixun Shang, Jincheng Wang, Hui Wang, Xianfeng Chen, and Xiaohong Zhang**

Prof. X. J. Zhang, Prof. J. S. Jie, W. Deng, Q. X. Shang, J. C. Wang, H. Wang, L. M. Huang, Prof. X. H. Zhang
Institute of Functional Nano & Soft Materials (FUNSOM)
Collaborative Innovation Center of Suzhou Nano Science and Technology (NANO-CIC)
Jiangsu Key Laboratory for Carbon-Based Functional Materials & Devices
Soochow University
Suzhou Jiangsu 215123, P. R. China.
Dr. Xianfeng Chen
School of Chemistry and Forensic Sciences
Faculty of Life Sciences, University of Bradford
United Kingdom, BD7 1DP
E-mail: jsjie@suda.edu.cn, xhzhang@mail.ipc.ac.cn

Keywords: small-molecule organic seminconductor micro/nanocrystals, alignment and patterning, device applications

1. Introduction

Small-molecule organic semiconductor micro/nanocrystals (SMOSN) have recently aroused increasing interests due to their unique properties and prospective applications in high-performance and low-cost flexible electronic and optoelectronic devices.[1-8] They demonstrate many advantages that can complement or rival those of their inorganic semiconductor nanocrystals counterpart, such as favorable flexibility, tunability in electronic and optical properties,[7,9-13] compatibility with large-area, low-cost and low-temperature solution-processed methods like coating[4] and printing.[14] In addition, SMOSN also exhibit much better device performance than their corresponding amorphous or polycrystalline thin films, because highly crystalline SMOSN possess fewer undesirable grain boundaries and lower density of defects, which can largely suppress the recombination of the excitons and thus accelerate effective charge transport.[15-18] Up to now, various techniques have been developed for the growth of SMOSN,[19] including solvent exchange method,[20] evaporation-induced self-

assembly method,[21] vapor deposition method[6,22] and template method.[23,24] Electronic and optoelectronic device applications like photodetectors,[25-28] organic field-effect transistors (OFETs),[6,8,14-17,29] and organic light emission diodes,[30] have also been successfully demonstrated.

Despite of all these advantages, the scale-up of SMOSN for practical industrial applications is still difficult because the growth orientation and location of SMOSN are usually stochastic in nature. Additionally, it has been confirmed that charge anisotropy exists in organic molecular crystals,[31,32] which means SMOSN will exhibit different electrical properties at different orientations. Thus it is prerequisite for SMOSN to be well-aligned to avoid device-to-device variation in performance, which is essential for their practical applications. Large-scale high-integration industrial applications such as active matrix displays, logic circuits, and sensor arrays require excellent device uniformity and reproducibility as well as minimal cross-talk between neighboring devices.[33,34] Therefore, SMOSN need to be well patterned at desired locations or selectively grown where the electrodes are located.[24,35,36] Overall, the ability of large-area alignment and patterning of SMOSN is indispensable for the realization of the integrated devices and circuits.[37] The development of alignment and patterning techniques will facilitate the practical application of SMOSN and enhance their device performance.[4,38,39]

Unlike their inorganic and macromolecular counterparts, SMOSN are constituted by weak non-covalent bonding interactions like hydrogen bonding, π-π stacking, dipole-dipole interactions and van der Waals forces.[40] Thus, they are usually chemically and mechanically fragile, resulting in the tendency to be easily damaged at high mechanical strengths, high temperatures or in organic solvents. Thus, conventional patterning techniques for inorganic materials cannot be simply applied to SMOSN. For example, as a mature and powerful patterning technique, photolithography has been widely adopted in current electronic industries because of its high reliability, resolution, accuracy, flexibility and capability for wafer-scale production.[41-43] However, it is not applicable for SMOSN, because most of the SMOSN cannot

tolerant the organic solvents that involved in photolithography processes.[44,45] As such, progress in the alignment and patterning of SMOSN is far behind their inorganic counterparts, which in turn impeds the development of their practical device applications.

Recently, great efforts have been devoted to develop strategies for assembling SMOSN into highly ordered arrays and desirable patterns at well-defined positions. Solution-processed methods including coating, printing and self-assembly based approaches have been reported for the fabrication of SMOSN arrays and patterns.[4,14,21,36,46,47] These solution-based techniques have obvious advantages, such as convenient for mass production, no requirements for expensive apparatus and harsh experimental conditions (high temperature or high vacuum etc), which will largely save the device cost. Another strategy is vapor-processed method, which usually involves heating organic materials at high temperature zone to produce molecular vapor, and then vapor transports downstream to low temperature region for crystal growth and assembly.[33] The assembly and alignment of the crystals are usually assisted by templates or external forces.[22,29,48,49] The distinct advantage of the vapor-based techniques is that the resulting crystals normally enjoy much better crystal quality than these produced from solution-based methods, which can guarantee better performance of the devices. Solution-based methods easily introduce contaminations (e.g., solvent molecules and impurities) into crystals during growth processes, which will weaken their corresponding electronic properties and thus impair the device performance.[50]

In this review, we will highlight recent progress in the strategies that developed for the alignment and patterning of ordered SMOSN within the past several years, the advantages and limitations of different methods are discussed, and the corresponding applications for various optoelectronic devices and integrated circuits are also summarized.

2. Solution-processed techniques for alignment and patterning of SMOSN

2.1. Self-assembly method

Self-assembly method has been widely used to fabricate one-dimensional (1D) SMOSN, which usually utilizes typical non-covalent bonding interactions (e.g., π-π interaction,[51] hydrogen-bonding interaction,[52-54] and dipole-dipole interaction[55]) between neighboring organic molecules to induce directional growth of SMOSN. However, the self-assembled SMOSN usually have disordered distribution, which commonly bring serious problems for large-area device fabrication and reduce the uniformity of device performance.[56-58] The alignment or patterning of self-assembled SMOSN often needs external forces to guide the process, such as evaporation-induced surface tension,[21,26,59,60] template,[23,24,61-71] wettability,[72-77] and electric/magnetic-field[78-83].

2.1.1. Evaporation-induced self-assembly at interfaces

Zhang and coworkers have demonstrated the use of evaporation-induced surface tension at liquid-solid or liquid-liquid interface to guide one-step growth and alignment/patterning of SMOSN (**Figure 1**).[21,26,59,60] Solution evaporation on a horizontal solid substrate will produce concentric rings of highly ordered nanowire (NW) arrays, while evaporation on a vertical substrate results in parallel stripes of NW arrays (Figure 1a-c). The alignment and patterning of NWs is induced by the mechanism of "coffee ring effect".[21] The schematic mechanism is presented in Figure 1d. At the beginning, the solvent is pinned on the substrate surface with a contact angel of θ_0, forming contact line due to surface roughness. With the evaporation of the solvent, organic molecules gradually precipitate out to form nuclei/aggregates along the contact line, which makes growth of the 2,4-bis[4-(N, N-dimethylamino)phenyl]squaraine (SQ) NWs starting at the same line. After that, due to the

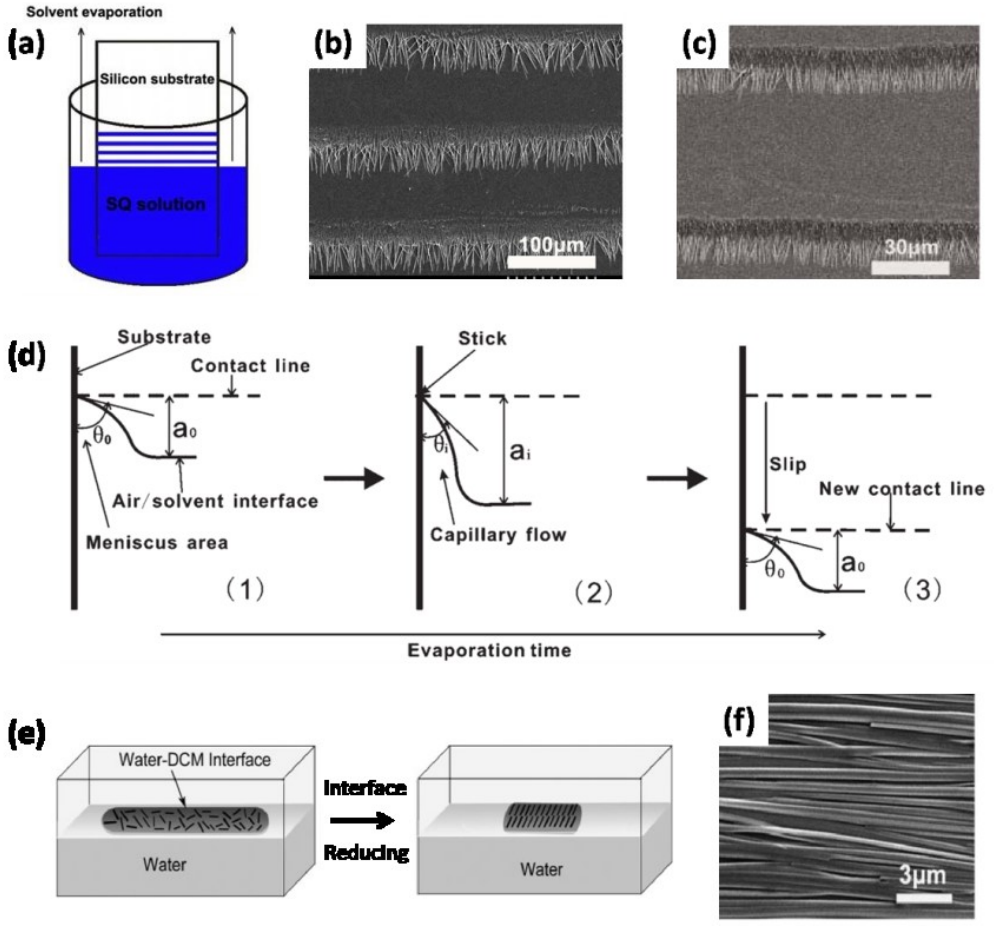

Figure 1. (a) Schematic illustration of evaporation-induced self-assembly on a vertical substrate. (b,c) SEM image of aligned parallel stripes of SQ NWs and PDI NWs on a silicon substrate, respectively. (d) Schematic illustration of the contact line moving process on a vertical substrate induced by solvent evaporation. (a-d) Reproduced with permission.[21] Copyright 2008, Wiley. (e) Schematic illustration of the evaporation-induced self-assembly at liquid-liquid interface. (f) SEM image of the aligned NW array film formed from SQ/DCM solution at liquid-liquid interface. (e-f) Reproduced with permission.[59] Copyright 2009, Wiley.

concentration gradient, additional molecules will flow toward the growing sites (contact line), where they will gradually self-assemble into 1D NWs driven by directional intermolecular interactions among neighboring molecules. During the growth process, tips of the NWs are controlled by the flow of the solution, thus the alignment of the NWs is achieved simultaneously

along the solution dewetting direction. With the solvent evaporation, the contact angle reduces ($\theta_i < \theta_0$) and the meniscus interface area goes up ($a_i > a_0$), leading to an increase in depinning force, with the pinning force remaining constant. Once the depinning force becomes larger than the pinning force, the contact line will jump to a new position and start another circle of NW growth and alignment. This facile method also allows the growth of aligned arrays of other organic materials, such as N,N'-di(1-octyl)perylene-3,4,9,10-bis(dicarboximid) (PDI) and bis(di-methylglyoximato)-nickel ($Ni(DMG)_2$) (Figure 1c).

In addition, evaporation-induced self-assembly at liquid-liquid interface can also induce the aligned/patterned growth of single-crystalline NWs.[59] The schematic illustration of this approach is shown in Figure 1e. A solution of SQ/dichloromethane (DCM) was put into a vessel and then a small amount of water was added onto the surface. With the evaporation of DCM, SQ molecules first grew into NWs at the interface and then gradually self-organize into parallel-aligned structures driven by the surface tension induced from the shrinkage of the DCM-water interface. With the completion of evaporation, a compact aligned NW film was left behind, floating on the water surface, which can be easily transferred to any desired substrate for further device applications (Figure 1f). This one-step method takes advantage of the nature of evaporation to narrow the liquid-liquid interface and thus induces the simultaneous growth and alignment of organic NWs. The mechanism behind this alignment method is quite similar with the conventional Langmuir-Blodgett (LB) technique, where the surface pressure that makes NWs in parallel-aligned arrangement is offered by external applied forces (e.g., mechanical brush).[59] This method of evaporation-induced alignment at liquid-liquid interface is also applicable to fabricate many other aligned organic NW array films such as Zn(salophen) and $Ni(DMG)_2$.

2.1.2. Template-guided self-assembly

Template-guided self-assembly methods use a template to induce the alignment/patterning of SMOSN, which, besides alignment, offer additional advantages of controlling the position and orientation as desired and capability of large-area fabrication. Without a template, the solution evaporation process is free to extend over the entire substrate/area and thus it is hard to achieve precise control of the alignment/patterning process. The underlying force that directs the alignment/patterning of NWs in template-guided methods is the capillary force.[23,24,61-71]

Template-guided self-assembly methods can be divided into two categories. In both cases, the capillary force first draws the solution flow toward the template. After that, in one strategy, the template acts as the stamp/mold to "print" out NWs with alignment/patterns copying that of the template. Elastomeric poly(dimethylsiloxane) (PDMS) with periodic lines (or shapes) has been mainly adopted as the template, due to its ease fabrication and design features.[61-64] In the other strategy, the template guides the alignment/patterning of NWs by controlling the solution flow direction during self-assembly processes of NWs with solvent evaporation.

In the first strategy, a PDMS stamp is usually used as the template, which is pre-developed by micro/nano fabrication technology (e.g., nanoimprint lithography) with defined channel width, intervals and patterns.[61,62] It has been reported that the PDMS stamp can induce the formation of perylene derivative (n-type organic semiconductor) NW arrays across the gold (Au) electrodes.[61] **Figure 2**a gives the schematic illustration of the process. The PDMS mold with regular parallel protrusions is placed directly on the substrate bearing with Au electrodes, which separate the PDMS channels away from the substrate surface. When a solution is dropped at one side of the PDMS template (perpendicular to the channel direction), capillary force will attract the solution to flow inside along the gap between the substrate and the PDMS. Upon the solvent evaporation, the solution is pinned just

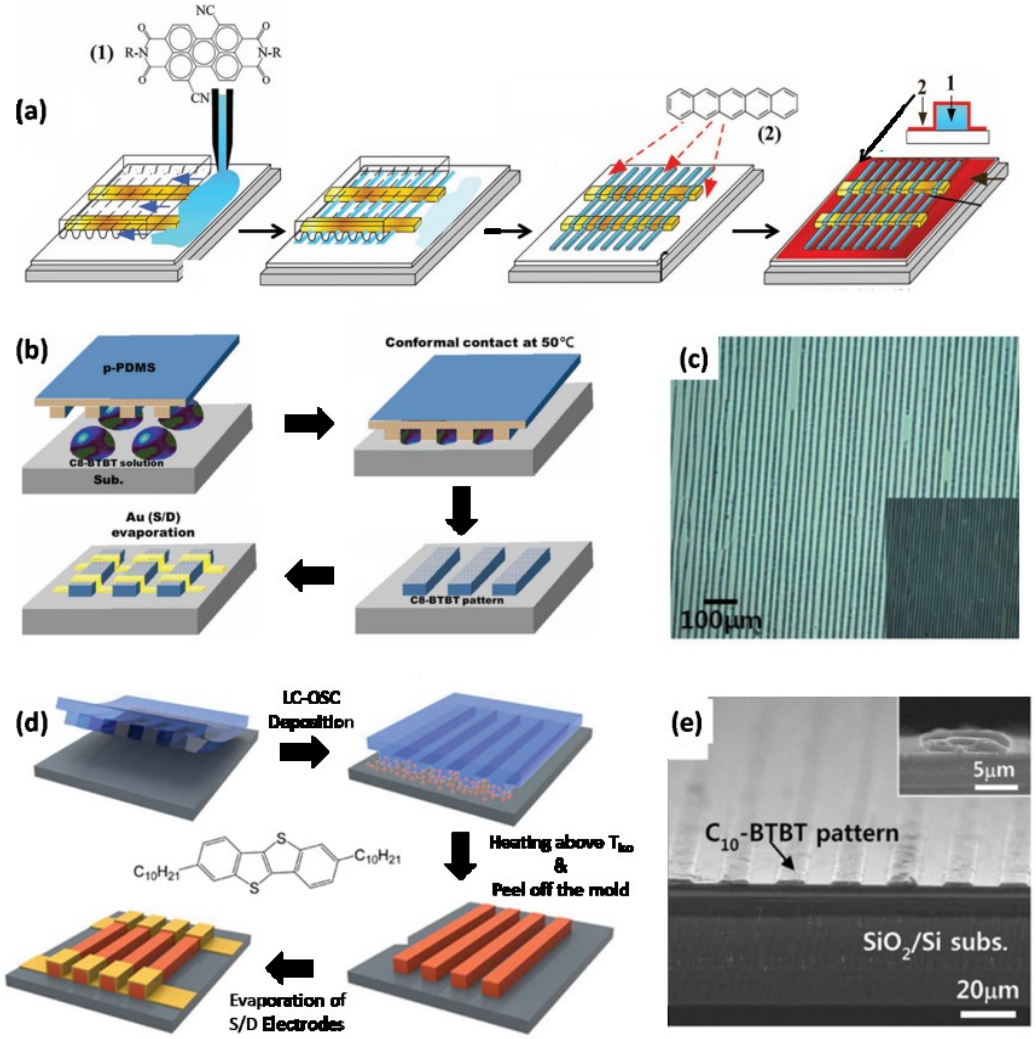

Figure 2. (a) Schematic illustration of the formation of perylene derivative NW arrays across the gold electrodes by using PDMS mold with regular parallel protrusions. (a) Reproduced with permission.[61] Copyright 2011, Wiley. (b) Schematic illustration of the micropattern fabrication process. (c) Optical micrograph of C_8-BTBT lines prepared by template-guided self-assembly method. (b-c) Reproduced with permission.[63] Copyright 2012, Wiley. (d) Schematic illustration of the highly ordered arrays of C_{10}-BTBT by using the PDMS as the topographic template. (e) The cross-sectional SEM image of C_{10}-BTBT line patterns prepared on the SiO_2/Si substrate, inset is the magnified cross-section image of a line pattern with internal layered structure. (d-e) Reproduced with permission.[64] Copyright 2013, Wiley.

under the template protrusions, and the molecules are then deposited out to form nuclei. With additional solutions continuously flowing towards the nuclei, aligned micro- or nanostripes will be gradually formed along the protrusions via self-assembly. It should be noted that nanostripes are not formed inside the channels but between the template protrusions and the substrate. With this method, after an n-type semiconductor nanostripe arrays were printed on the substrate, a thin film of p-type semiconductor (pentacene) can then be thermally evaporated on the top of stripes, forming a planar ambipolar multi-stripe OFET. Similarly, a so-called nanomolding in capillaries (NAMIC) method was also proposed to fabricate various nanopatterns by using PDMS as a template.[62] In order to prevent the swollen of the PDMS template, material was first dissolved in a polar solvent to make a solution. After PDMS template was put on the substrate, the solution was dropped at the edge of the mold. The capillary force would drive the solution flow towards the mold. Upon solvent evaporation, organic materials deposited out to form NW arrays on the substrate within the confinement of the channels. After the mold was peeled off, aligned stripes with controlled orientation were left on the substrate. Based on this technique, various nanopatterns including poly(3,4-ethylenedioxythiophene) doped with poly(styrene sulfonate) (PEDOT:PSS), SiO_2 nanoparticles (NPs), and organic dye tetramethylrhodamine isothiocyanate (TRITC) were successfully fabricated, demonstrating the generality of this method.

As another example, as shown in Figure 2b, dioctylbenzothienobenzothiophene (C_8-BTBT) solution (2 wt% 1,2,4,5-tetrachlorobenzene (TCB)) was directly drop-cast on the substrate and then PDMS template was placed upon the substrate, making it having intimate contact with the droplets of C_8-BTBT solution.[63] Then the solution was annealed at 50 °C for 4 hours to solidification. During the process, capillary force drived the solution flow towards the concave channels, where C_8-BTBT molecules were precipitated out to form nanostructures. The wall of nanochannels offered nucleation sites for oriented growth of nanopatterns within the confinement of the template. After the detachment of the PDMS template, C_8-BTBT nanoline

arrays were produced on the substrate (Figure 2c). The width, interval spacing and dimensions of the patterns can be controlled by those of the PDMS template. Crystal structure analysis indicated that C_8-BTBT crystals were oriented along [100] direction. This technique also allows the fabrication of grid patterns of C_8-BTBT NWs. Based on the line patterns, the authors further fabricated top-contact OFETs, which exhibited good electronic performance with an average mobility of 0.9 $cm^2 V^{-1} s^{-1}$. Recently, highly ordered arrays of liquid crystalline molecules were also fabricated from their powders by using PDMS as the topographic template.[64] The formation process is illustrated at Figure 2d, the crystalline 2,7-dide-cylbenzothienobenzothiophene (C_{10}-BTBT) powder was placed at the entrance of the trenches and then heated over 122 °C (the isotropic phase temperature of C_{10}-BTBT). During the treatment, the capillary force will drive the isotropic liquid phase of C_{10}-BTBT flow into the channels of PDMS template until they are filled with C_{10}-BTBT. After that, the C_{10}-BTBT was cooled down to room temperature and PDMS template was detached from the substrate, highly ordered arrays of C_{10}-BTBT lines were produced on the substrate (Figure 2e).

In the second strategy of template-guided self-assembly method, the template does not simply serve as a mold but provides a guidance to control the solution flow direction and the contact line formation during solvent evaporation. In crystal growth process, the spatial confinement effect of the template can force crystal growth along a specific direction or at desired locations. Templates like silicon wafer, glass stylus and covering hat have been demonstrated to induce the formation of ordered SMOSN patterns.[24,65-68] A silicon wafer has been reported to be used as the template to pin the solution and control its flow direction.[24,65-67] The schematic illustration is shown in **Figure 3**a and 3d. Upon evaporation, the droplet shrinked with solution receding direction toward the center of the template. The solution flow directed the subsequent aligned and patterned growth of NWs. Once the solution was full evaporated, NW array patterns would be formed surrounding the silicon wafer

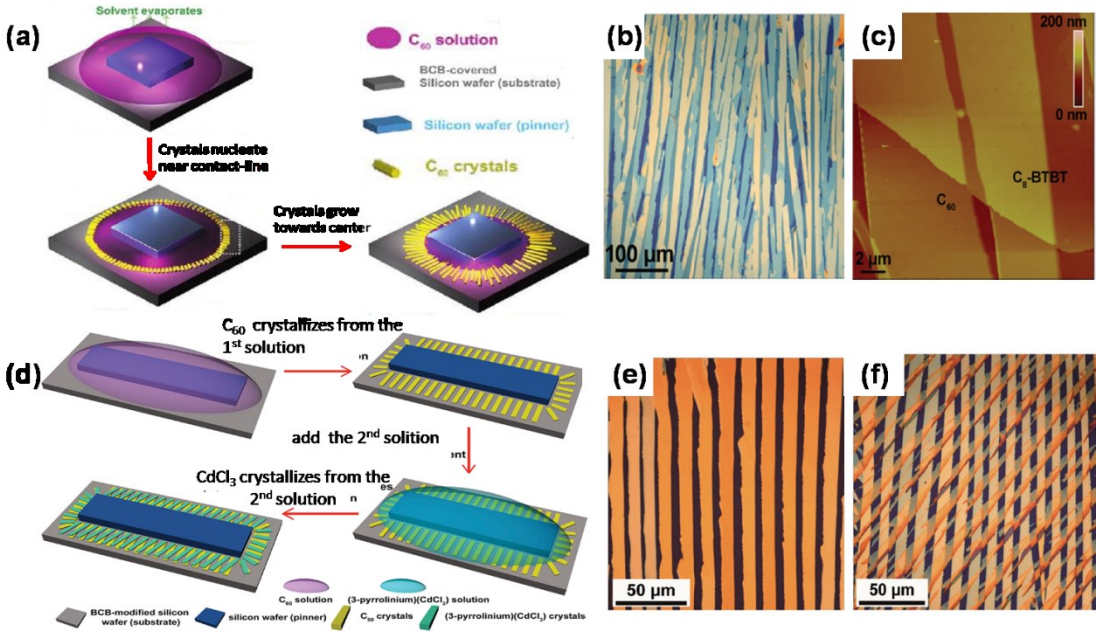

Figure 3. (a) Schematic illustration of the silicon wafer guided self-assembly process for the formation of p-n junction NW arrays from a mixture solution of C_8-BTBT (p-type) and C_{60} (n-type). (b) Optical micrograph image of as-prepared C_8-BTBT ribbon and C_{60} ribbon p-n junctions. (c) An AFM image of the p-n junction. (a-c) Reproduced with permission.[66] Copyright 2013, Wiley. (d) Schematic illustration of two-step crystallization process based on the silicon wafer guided self-assembly method. (e) Optical microscopy image of C_{60} NW arrays. (f) Optical microscopy image of the bilayered structure. (d-f) Reproduced with permission.[67] Copyright 2015, Wiley.

with NW tips pointing toward the center of the silicon wafer. By using silicon wafers with different shapes, various NW array patterns like square, rectangle and circle have been obtained.[24] The method is also applicable to many other SMOSN, such as 6,13-bis(triisopropyl-silylethynyl) pentacene (TIPS-PEN). With this technique, single-crystalline organic p-n junction arrays were also fabricated from a mixture solution of C_8-BTBT (p-type) and C_{60} (n-type) (Figure 3b,c). Importantly, high-performance transistors with ambipolar charge transport characteristics were successfully demonstrated based on these aligned NW

arrays.[66] Similarly, Wu and co-workers reported the growth of ferroelectric 3-pyrrolinium)($CdCl_3$) NW arrays onto C_{60} NW arrays by using a two-step crystallization process and achieved high-performance memory devices.[67] The schematic growth process is shown in Figure 3d, a drop of C_{60} solution was firstly applied on the substrate with a silicon wafer as the template. C_{60} NW arrays were then formed during the solvent evaporation (Figure 3e). Subsequently, addition of another solution of inorganic material ((3-pyrrolinium)($CdCl_3$) in ethanol) led to the formation of new layer of inorganic NW arrays on the top of C_{60} NW arrays, resulting in a bilayered structure (Figure 3f). The OFET-based memory devices were fabricated based on the resulting bilayered single crystal arrays, excellent memory performance and a high electron mobility of 1.28 ± 0.41 cm^2 V^{-1} s^{-1} were obtained.[67] A glass capillary tube was also demonstrated as a template to induce the solution flow for the formation of NW arrays of perylene diimide derivative on both sides of the tube.[68]

Besides in-plane templates, three-dimensional steric templates are also reported to confine the solution evaporation within a specific space for the following growth of various NW array patterns.[23,69-71] Wang *et al* applied a spherical lens to serve as a spatial template to confine N,N'-Dimethylquinacridone (DMQA) solution evaporation as shown in **Figure 4**a. Using this method, the authors obtained regular concentric rings of ordered and aligned organic NWs.[23] The spherical lens provides a restricted space for controlling the flow and the spatial restriction causes the deposition of NWs in a much more controlled manner. As the solution slowly shrinks upon evaporation, evaporation-induced capillary force drives the flow toward the central template–substrate contact region, which induces the aligned growth of NWs (Figure 4b,c). Shape of the contact line is determined by the geometry of the edge of the solvent pool between the template and substrate. Various parameters including shape, curvature radius of the covering hat, and substrate type were further systematically investigated to study their influence on the fabrication of NW arrays.[69] A surface-tension model was also put forward to elaborate on the interaction of the solution with the covering hat and substrate during evaporation process (as

shown in Figure 4d). By tuning the geometry of the covering hat, square- and triangular-patterns of

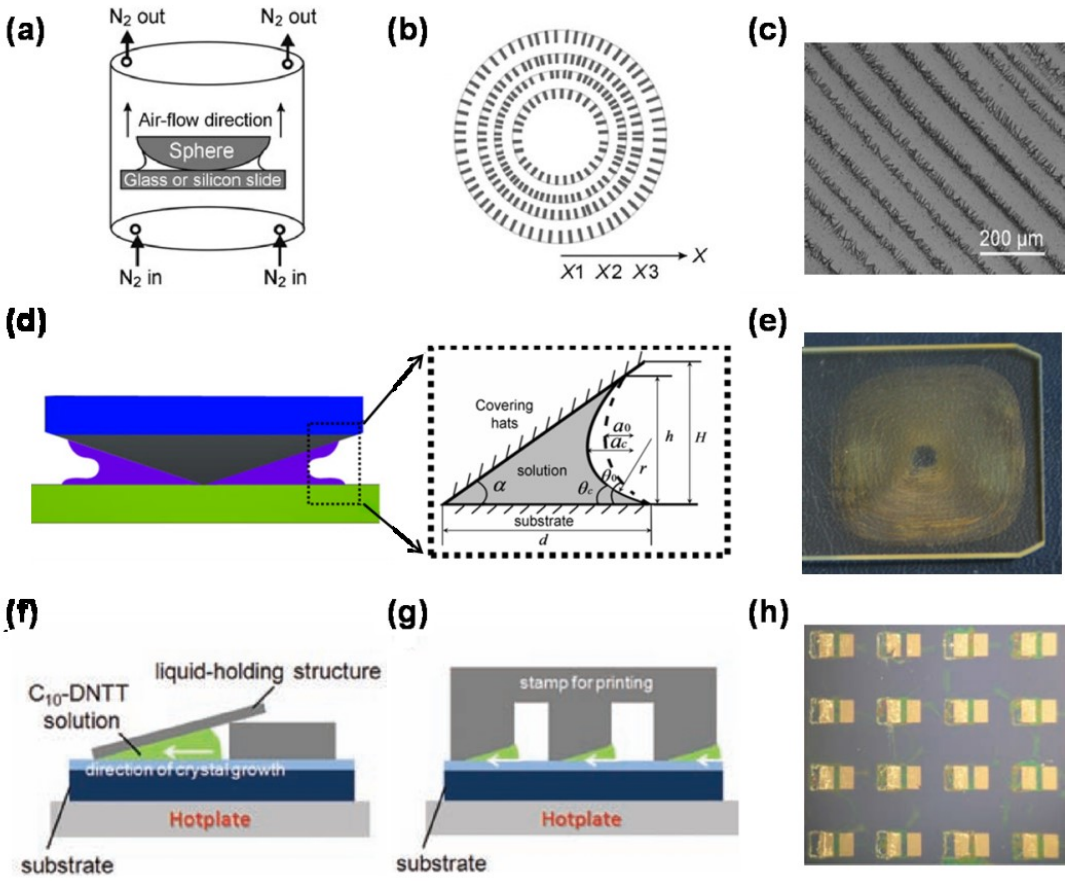

Figure 4. (a,b) Schematic illustration of the sphere-on-flat evaporation process and the resulting concentric rings of organic NWs. (c) Optical micrograph of the concentric rings of DMQA NWs formed during solvent evaporation. (a-c) Reproduced with permission.[23] Copyright 2011, Wiley. (d) Schematic illustration of the interaction between the solution with the substrate and the covering hat. (e) Optical image of NW arrays fabricated by a square rectangular pyramid as the template. (d-e) Reproduced with permission.[69] Copyright 2012, Wiley. (f,g) Schematic illustration of the fabrication of NW arrays by using a stamp template with an inclined slope. (h) An optical microscopy image of the as-prepared transistor arrays. (f-h) Reproduced with permission.[71] Copyright 2011, Wiley.

NW arrays with varied periodicity and NW density were developed on different substrates (Figure 4e). Glass stylus has also been used to direct the outward capillary flow for the fabrication of TIPS-PEN NW arrays, which is driven by confined solvent evaporation within the space between curved upper surface and the flat lower substrate.[70] Solvent type and substrate surface energy were found to have great influence on the morphologies of the resulting NW arrays. Recently, a template with an inclined slope was demonstrated to control the solution evaporation for the growth of crystalline film arrays at intended positions.[71] As illustrated in Figure 4f, a template with an inclined slope was placed on the substrate. Solution was directly introduced into the gap area and then heated to approximately 100 °C. With the solvent gradually drying, crystalline film was continually grown along the solution motion toward the closed edge. This strategy allows the deposition of crystalline film directly across the gold electrodes on the substrate (Figure 4g,h), therefore, matrix transistor arrays can be simultaneously fabricated. This method holds the advantage of having the capability of fabricating separated device arrays in one-step, but one concern is that the produced device arrays usually featured with large size (hundred micrometers or more) and relatively low space resolution. Hence, it needs to be further improved for applications in large-scale integrated circuits.

2.1.3. Wettability-guided self-assembly

Wettability-guided self-assembly process commonly utilizes substrate wettability to control the growth location of SMOSN. Surface regions modified by alkyl or fluoroalkyl groups display nonwettable property with poor solvent residual affinity, while those functionalized by phenyl groups show favorable surface for deposition of organic materials.[72-77] Zhang *et al.* described the formation of aligned organic NW arrays at desired positions on substrate with controlled patterns of surface wettability.[72] As illustrated in **Figure 5**a, the substrate was first treated by octadecyltrichlorosilane (OTS) to produce a nonwettable film on the substrate surface and then ultraviolet (UV) irradiation was applied onto the OTS-modified film through a shadow mask.

Through the illumination, the exposed area became wettable. When the evaporation-induced self-assembly process was performed on the wettability-patterned substrate, organic nanostructures were then observed to grow preferentially on the solvent wettable regions with controlled alignment.

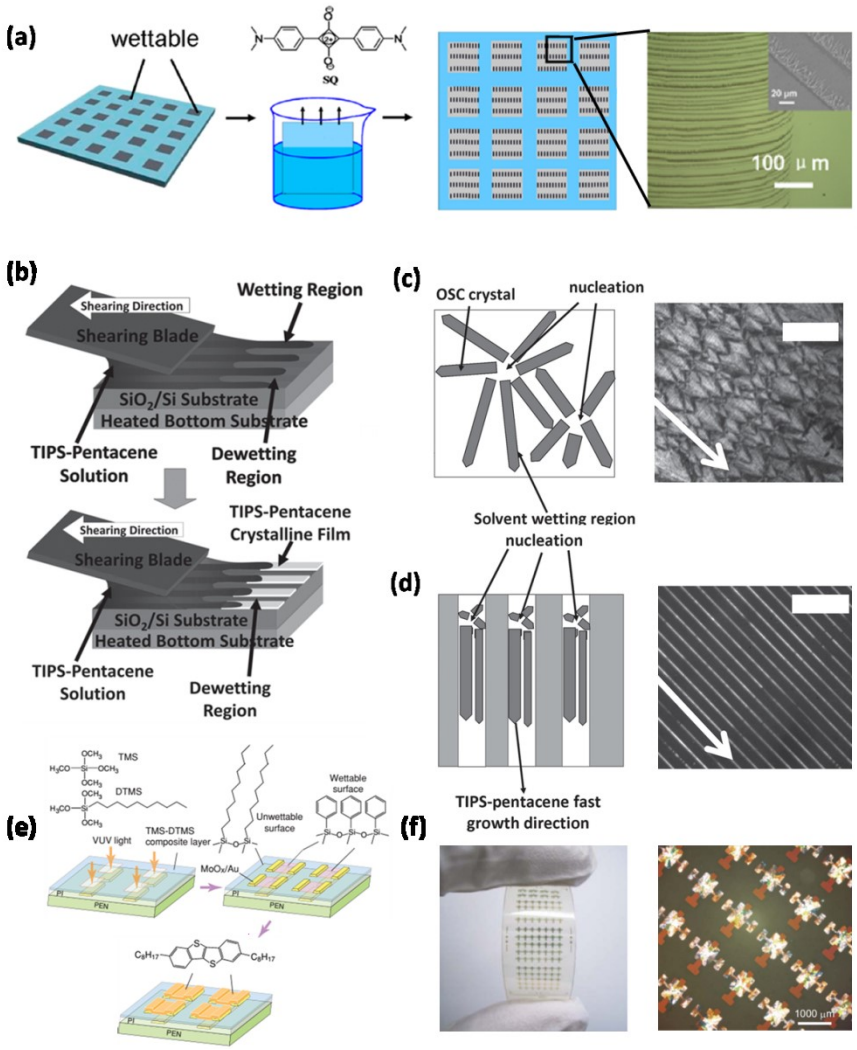

Figure 5. (a) Schematic illustration of wettability-guided self-assembly process of organic materials for the growth of aligned NW arrays by using a solvent evaporation method. (a) Reproduced with permission.[72] Copyright 2013, American Chemical Society. (b) Schematic illustration of the formation of TIPS-PEN NW arrays on the wettability-patterned substrate by using a blade-coating method. (c,d) Schematic illustration of the selective growth of TIPS-PEN at wettable lines with controlled alignment and the corresponding cross-polarized microscopy images. Scale bars are all 25 μm. (b-d) Reproduced with permission.[73] Copyright 2014, Wiley.

(e) Schematic illustration of the fabrication process of NW arrays selectively on electrode areas on a flexible substrate. (f) Photograph of flexible transistor matrix composed of self-organized OFETs. (d-f) Reproduced with permission.[77] Copyright 2009, American Institute of Physics.

Wettability-guided self-assembly process is often combined with other technologies for patterning.[73-77] By using a blade-coating method, highly aligned TIPS-PEN crystalline film was found to preferentially grow on wettable regions on a substrate with alternating solvent wetting/dewetting lines (Figure 5b).[73] TIPS-PEN displayed unaligned growth on the unpatterned substrate (Figure 5c). In contrast, when the substrate was patterned with solvent wetting/dewetting lines, TIPS-PEN crystals selectively grew along the wettable lines with controlled alignment toward the receding direction of the blade (Figure 5d). In another example, a plastic substrate bearing with gate electrode and insulator layer was selectively modified into wettable and nonwettable areas by use of silane self-assembly monolayers (SAMs). Then source and drain electrodes were deposited onto the wettability-controlled patterned insulator surface through a shadow mask. After that, a semiconductor solution was dropped onto the substrate. The solution was observed to be attracted only to the wettable areas, leading to patterned growth of organic micro/nanocrystals arrays between electrode channels (Figure 5e). Device arrays were thus formed according to the patterned areas (Figure 5f). The resulting device was separated from each other, which effectively reduced the possibility of gate leakage current and crosstalk among devices.[33,34] In addition, growth of organic crystal arrays on a wettability-patterned substrate can also be achieved by combining with a spin-coating method,[74,76] which will be discussed in detail in the following “spin-coating” section.

2.1.4. Electric/magnetic-field guided self-assembly

When molecules exhibit an anisotropic dipole or magnetic moment, it is possible to control their alignment using electric or magnetic field.[78-83] Electric/magnetic-field guided self-assembly can induce the growth of SMOSN with controlled orientation at desired position. For example, electric field has been demonstrated to control the growth orientation and position of pentacene single crystals.[78] The process is schematically shown in **Figure 6**a. When an alternating electric field was applied between two electrodes, the polarized pentacene microcrystals would interact with it and produce dielectrophoretic (DEP) force. The DEP force could then drive pentacene microcrystals to deposit between two electrodes and grow along the electric field lines, bridging the two electrodes (Figure 6b). Similarly, electric field was also reported to be used to direct the self-assembly of fluorinated phenylbithiophene derivative with negative dielectric anisotropy to form aligned fibrous aggregates between electrodes.[79,80] It was found that, without the application of electric field, randomly entangled fibers were produced. Moreover, a phenylbithiophene derivative without fluoro substituents formed unaligned fibers even under an electric field, indicating the important role of the dielectric anisotropy nature of molecules in the patterning process.

Recently, Jie group demonstrated the use of electric field to assemble organic microcrystals into various patterns with assistance of photolithography.[81] As illustrated in Figure 6c, an aqueous suspension of perylene derivative microcrystals was first sandwiched in an indium tin oxide (ITO) glass cell. Then an electric field was applied normally to the two ITO glass electrodes, crystals quickly moved to the bottom electrode surface and assemble into desired patterns in exposed ITO areas by optimizing frequency and electric field strength. Combined with photolithography patterning technique, shapes of the assembled patterns can be precisely controlled by the lithographic bottom pattern geometries (Figure 6d). Patterns with complex structures can be easily achieved as shown in Figure 6e. It is worth to note that the assembly of these crystals is driven by electrohydrodynamic flows generated by the electric field, which is

quite different from that of other electric-field induced self-assembly processes, where the DEP force plays a critical role in crystal alignment.

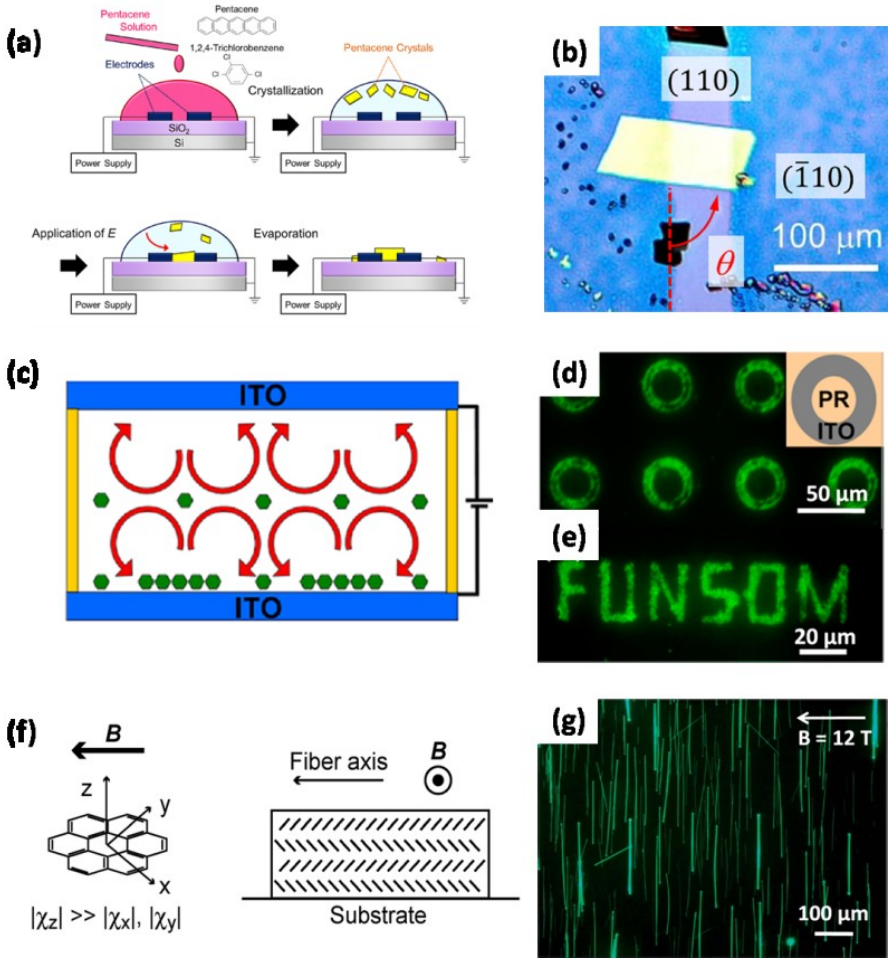

Figure 6. (a) Schematic illustration of the electric-field guided self-assembly of pentacene microcrystals between the two electrodes. (b) Optical image of a pentacene single crystal bridging the two electrodes. (a,b) Reproduced with permission.[78] Copyright 2014, American Chemical Society. (c) Schematic illustration of the electric-field guided patterning of organic nanocrystals driven by electrohydrodynamic flow in the ITO glass cell. (d) Fluorescence microscopy image of the patterns formed on the ITO substrate with circular photoresist patterns. Inset is the corresponding as-prepared photoresist patterns on the ITO substrate. (e) Fluorescence microscopy image of the complex patterns of "FUNSOM". (c-e) Reproduced with permission.[81] Copyright 2014, American Chemical Society. (f) Left is diamagnetic susceptibility of a coronene molecule. The axis of the largest diamagnetic susceptibility (Z axis)

is perpendicular to the aromatic disc plane. The $\boldsymbol{Z} \perp \boldsymbol{B}$ orientation exhibits the lowest magnetic energy. Right is the crystal structure of a coronene nanofiber. Black bars give side views of coronene molecules. (g) Fluorescence microscopy image of magnetically aligned nanofibers. (f,g) Reproduced with permission.[82] Copyright 2014, The Royal Society of Chemistry.

Another route for patterned/aligned growth of SMOSN is to use magnetic field to guide the self-assembly process (Figure 6f,g). As one example, single-crystalline coronene nanofibers have been prepared by applying a magnetic field.[82] Coronene molecules exhibit anisotropy in diamagnetic susceptibility due to their highly ordered internal molecular arrangement. When a magnetic field is applied, they tend to orient in a direction perpendicular to the magnetic field direction to minimize the magnetic energy, as illustrated in Figure 6f. It was observed that the resulting nanofibers were highly aligned perpendicular to the magnetic field direction (Figure 6g). The mechanism is believed to be the anisotropy of the diamagnetic susceptibility of coronene molecules and the crystal structure of the formed nanofibers. Highly ordered 2,3-bis-n-decyloxyanthracene fibers with orientation perpendicular to the magnetic field direction, were also fabricated by using this magnetic alignment mechanism.[83]

2.2. Coating

Coating is a commonly used industrial technique for deposition of uniform organic thin films.[84-91] Typical coating methods include dip-coating, spin-coating and blade-coating. In this section, we will introduce and discuss their applications in the fabrication of ordered organic micro/nanocrystal arrays.

2.2.1. Dip-coating

Dip-coating is a widely used method to fabricate organic crystalline micro/nanostructures with aligned features.[92-96] In a dip-coating process, a substrate is immersed into a solution of coating materials and then pulled up from the solution at a controlled speed. With solvent evaporating from the liquid on the substrate, organic micro/nanocrystals will be formed through self-

assembly process.[97-100] Tips of self-assembled organic micro/nanocrystals are directed along the pulling direction, resulting in the alignment of ordered arrays. Properties of the formed nanostructures like shape and thickness can be tuned by various

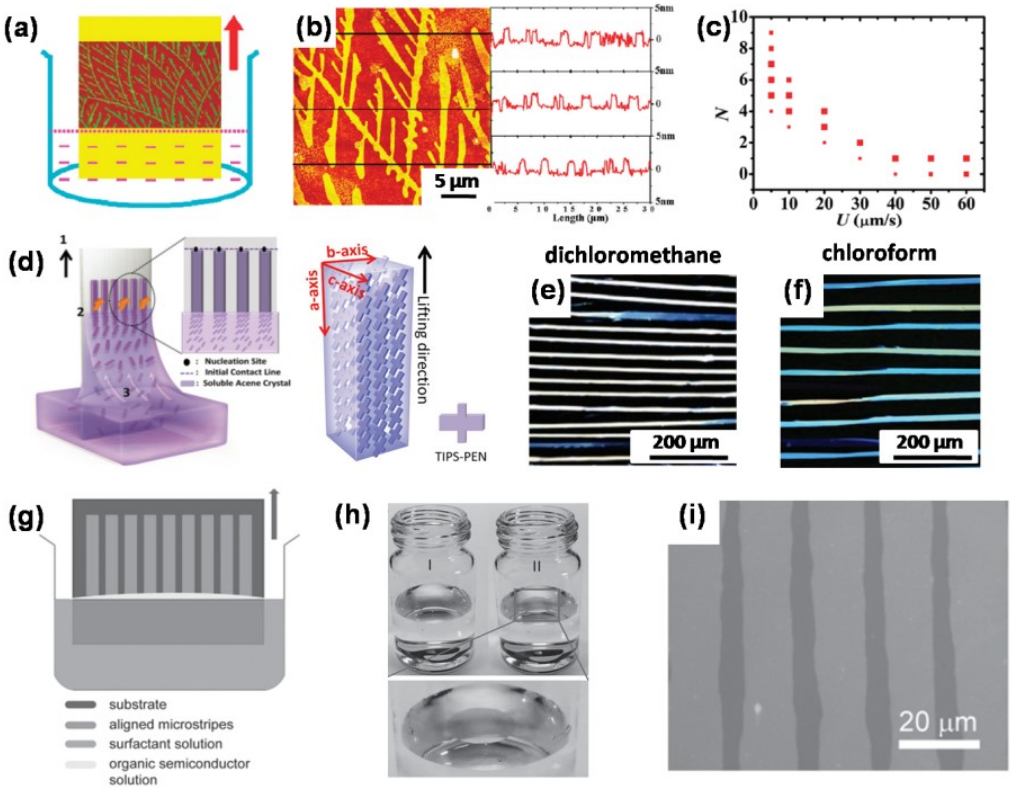

Figure 7. (a) Schematic illustration of dip-coating process. (b) AFM image of monolayer microstripe and height profiles from different areas. (c) The number of molecular layers (N) of microstripes as function of pulling speed. (a-c) Reproduced with permission.[101] Copyright 2010, American Chemical Society. (d) Schematic illustration of the crystal growth process by dip-coating method and their unite cell directions. (e,f) Cross-polarized optical microscope images of dip-coated TIPS-PEN crystals at pulling speed of 150 µm/s from dichloromethane (e) and 50 µm/s from chloroform (f), respectively. (d-f) Reproduced with permission.[46] Copyright 2012, Wiley. (g) Schematic illustration of the so-called two-phase dip-coating method. (h) Images of the aqueous surfactant solution (I) and two-phase solution (II). (i) Optical images of the microstripes dip-coated from two-phase solution. (g-i) Reproduced with permission.[103] Copyright 2014, Wiley.

parameters including pulling speed, environmental humidity, as well as solution composition, concentration and temperature.[46,92,100] Li and co-workers recently demonstrated the use of dip-coating method to achieve aligned growth of monolayer to multilayer microstripes of a prototype organic semiconductor by controlling the pulling speed (**Figure 7**a,b).[101] They systematically studied the relationship between pulling speed and the number of molecular layers and morphologies of the resulting microstripes. It was revealed that faster pulling speed resulted in thinner and more uniform layers. A pulling speed of over 40 μm/s yielded monolayer stripes, while multilayer stripes occured at a pulling speed of below 20 μm/s (Figure 7c). They further fabricated field-effect transistors based on the microstripes with controllable molecular layers and studied their charge transporting properties in the real charge accumulation and transporting layers. These as-prepared microstripes based OFETs could act as excellent ammonia sensors with fast response/recovery rate, high sensitivity and robust stability.[102] A similar study was also performed for the fabrication of highly aligned acene nanocrystal arrays with outstanding OFET mobilities via a dip-coating method (Figure 7d).[46] In the work, various influence factors in the dip-coating method were thoroughly studied. By optimizing solvent type, dip-coating temperature, and substrate pulling speed, the researchers discovered that optimal fiber-shaped crystal arrays grow at a pulling speed of 150 μm/s (50 μm/s) in the presence of solvents with low boiling point like dichloromethane (or chloroform) (Figure 7e,f). On the basis of the experimental results, they further clarified crystallization kinetics of organic molecules at the air-solution-substrate contact line.

Good solubility of organic semiconductors is essential for above-mentioned dip-coating process. However, a considerable number of organic semiconductors with excellent electronic properties have limited solubility. For these materials, their device applications usually can only be achieved by vacuum vapor deposition method. Recently, a so-called two-phase dip-coating method was proposed to assemble p- and n-type organic semiconductors with low solubility

into highly ordered microstripes.[103] As shown in Figure 7g,h, several drops of a saturated organic semiconductor solution (a thiophene-based oligomer in chloroform in the work) were added onto the surface of an aqueous surfactant solution. Although chloroform is heavier than water, surface tension will make it float on the surface of water. The two-phase solution was then formed since the two solutions are immiscible with each other. After aging for several minutes, dip-coating process was performed in the two-phase solution. Aligned strips were formed on the substrate at a proper pulling speed (Figure 7i). In a control experiment, organic semiconductor was dip-coated directly from the chloroform solution. Only very few crystals with random orientations were observed to deposite on the substrate under any tested dip-coating conditions, due to its limited solubility in chloroform. The authors also found that surfactant played a key role in the growth process of microstripes, which was considered to change the cohesive energy between organic molecules, and decide the following crystal growth facet and molecular crystallization. By using this method, they obtained several kinds of aligned microstripes and used them to fabricate OFET devices.

2.2.2. Spin-coating

Spin-coating method involves applying a small amount of solution at the center of a substrate and then rotating it at high speed to spread the coating material.[104-108] After solvent evaporation, uniform film is formed on the substrate. Spin-coating is usually used to deposit uniform thin films on flat substrates. Thus, for alignment and patterning of organic micro/nanocrystals, it is usually combined with other confinement technologies like selective surface wettability modification for patterning. Li, Tsukagoshi and co-workers used a spin-coating method to fabricate organic crystal arrays on wettability-patterned substrate.[74,109] The procedures are described in **Figure 8**a and 8b. The substrate surface was firstly coated with a thin layer of hydrophobic amorphous fluoropolymer (CYTOP) and then treated with O_2-plasma with a shadow mask covered, through which the substrate was differentiated into hydrophobic and hydrophilic areas. Subsequently, a mixed solution (C_8-BTBT and polymethylmethacrylate

(PMMA)) was spin-coated onto the modified substrate. The coating materaisl were then confined to hydrophilic areas (Figure 8b),

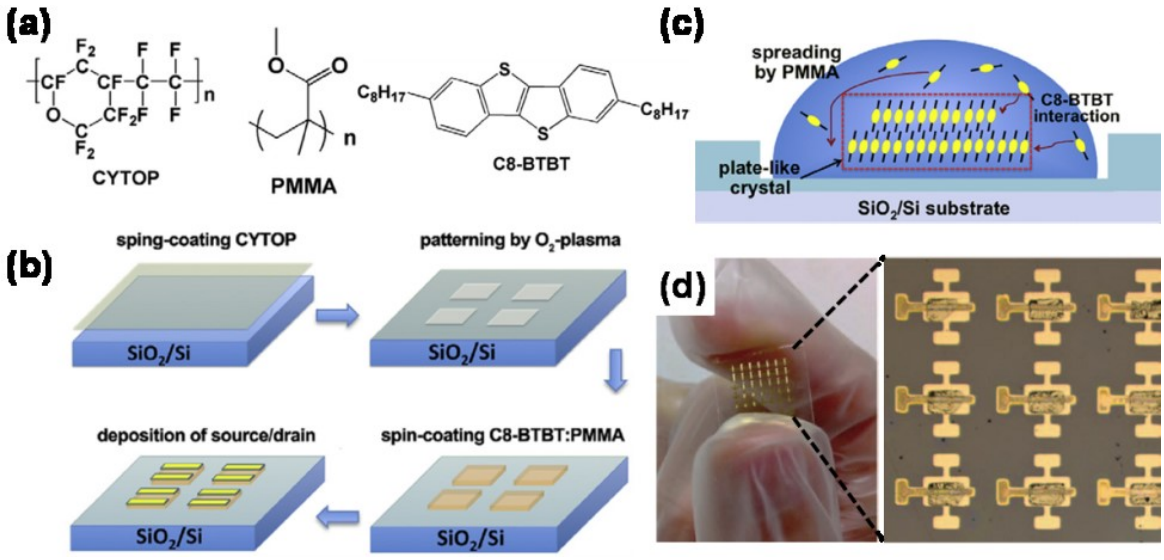

Figure 8. (a) Molecular structure of CYTOP, PMMA and C_8-BTBT. (b) Schematic illustration of the preparation process of organic crystal arrays on wettability-patterned substrate by using a spin-coating method. (c) Schematic illustration of the formation process of plate-like organic crystals with assistance of PMMA on the patterned wettable regions. (a-c) Reproduced with permission.[74] Copyright 2012, Elsevier. (d) The optical microscope image of a flexible polyethylene naphthalate (PEN) substrate with OFET device arrays fabricated by the proposed method. (d) Reproduced with permission.[109] Copyright 2013, American Institute of Physics.

resulting in selective deposition of plate-like C_8-BTBT microcrystals at desired locations after full solvent evaporation (Figure 8c,d). Spin speed and CYTOP-patterned layer have a great influence on the crystallinity and hence charge transport properties of the resulting organic structures. Low spin speed and the CYTOP layer greatly enhance the crystallization of organic materials in forming well-ordered structures and thus higher device performance. Without surface modification by CYTOP, a nonuniform film was produced, randomly distributing over the whole substrate with various-sized anisotropic crystalline structures.[110] In addition to

CYTOP, (tridecafluoro-1,1,2,2-tetrahydrooctyl)trichlorosilane (FTS) was also utilized to functionalize SiO_2/Si surface to be hydrophobic.[76] The substrate can then be patterned to having areas with different wettability after UV-ozone treatment with a shadow mask. After a solution was spin-coated onto the modified substrate, organic crystals selectively grew at electrode areas, thereby forming device arrays.

2.2.3. Blade-coating

Blade-coating technique is usually employed for depositing large-area organic semiconductor thin films, which uses a blade to drag the solution (ink) moving along one direction under a controlled rate on a rigid or flexible substrate. With the blade gradually receding and solvent evaporation, uniform organic micro/nanocrystal films are left behind on the substrate.[87,111-113] Compared with spin-coating method in which only a small portion of the solution is utilized, the advantage of blade-coating method is minimal solution wastage during coating.

Bao and co-workers used this method to fabricate highly aligned ribbon-like micro/nanocrystals of several organic semiconductors including TIPS-PEN, phenylene-dithiophene-phenylenes and phenylene-trithiophene-phenylene derivatives. The schematic process is shown in **Figure 9**a, a solution of organic material was first sandwiched between the blade and substrate. The motion of the blade exposed the liquid front to evaporate rapidly to produce nuclei. With the blade steadily receding, additional organic molecules continuously flowed towards the growing sites (nuclei), followed by self-organizing and growing preferentially to form aligned nanostructures. After blade-coating, uniform organic micro/nanocrystals were deposited with aligned direction parallel to the moving direction of the blade, extending over the entire substrate (Figure 9b-e). The following parameters were found to play key roles in the coating process: surface energy of the substrate, surface tension of the solution, surface temperature, solution concentration and coating speed. More importantly, it was also found that field-effect transistors based on these as-prepared organic micro/nanocrystals exhibited superior performance than that of those prepared from

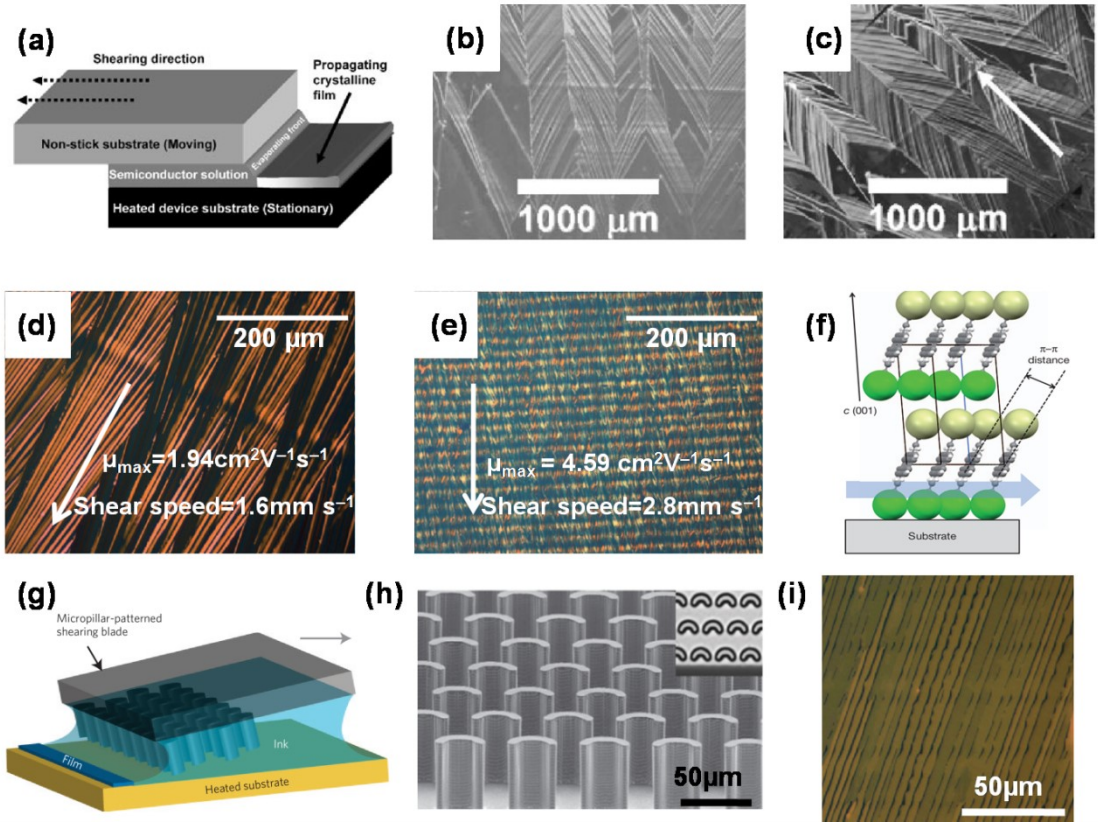

Figure 9. (a) Schematic illustration of the blade-coating method. (b,c) Bright-field optical micrograph and cross-polarized microscopy of the prepared NW films. The white arrow shows the blade-coating direction. (a-c) Reproduced with permission.[114] Copyright 2008, Wiley. (d,e) Cross-polarized optical microscope images of blade-coated TIPS-PEN thin films at coating speeds of 1.6 mm s^{-1} (d) and 2.8 mm s^{-1} (e). (f) Molecular packing structure of TIPS-PEN thin film at coating speed of 8 mm s^{-1}. (d-f) Reproduced with permission.[4] Copyright 2011, Nature Publishing Group. (g) Schematic illustration of blade-coating process by using a micropillar-patterned blade. (h) SEM image of a micropillar-patterned blade. The inset is top view of the micropillars under an optical microscope. (i) Cross-polarized optical micrograph image of the resulting TIPS-PEN film by using a micropillar-patterned blade at coating speed of 0.6 mm s^{-1}. (g-i) Reproduced with permission.[38] Copyright 2013, Nature Publishing Group.

drop-casting method.[114] High-resolution grazing incidence X-ray diffraction (GIXD) was further utilized to disclose the texture and molecular packing of organic micro/nanocrystals

obtained at different coating speed.[4] It was found that lattice strain was induced during the blade-coating process with increasing the coating speed, which could decrease the molecular packing distance, leading to closer π-π stacking and thus faster charge transport (Figure 9f). The optimal mobility can be as high as 4.6 $cm^2 V^{-1} s^{-1}$ for TIPS-PEN, which is twice higher than the best reported value (1.8 $cm^2 V^{-1} s^{-1}$) at that time. However, much higher coating speed will also result in grain boundary regions and domains with less oriented crystallites.[4,111] Based on these observations, another two strategies were proposed to further enhance the crystal quality of the resulting arrays. One is to modify the blade with silicon micropillars to induce recirculation in solution for improved crystal growth as shown in Figure 9g,h, the other is to pattern the substrate with alternating solvent wetting/dewetting lines to induce lateral confinement of crystal growth and lattice strain.[73] With these strategies, high-quality aligned crystals with enhanced mobilities were obtained accordingly (Figure 9i).[38]

2.3. Printing

Printing is a well-established patterning technique for organic electronics, which offers many promising advantages such as high throughput and adaptability to various kinds of substrates.[115,116] Inkjet-printing, transfer-printing and template-induced printing have been employed for alignment and patterning of SMOSN.

2.3.1. Inkjet-printing

Inkjet-printing is a highly effective patterning method, which usually includes storing ink in a chamber and then deposition of a quantitative solution from the chamber at intended locations via jet ejection. Once the ejected solution dries, crystals will be formed.[117] Inkjet-printing has become an important technology for organic electronic device applications, owing to its unique advantages like precise control of the volume of depositing solution and depositing location, efficient use of materials, and minimal contamination due to non-contact deposition process.[118]

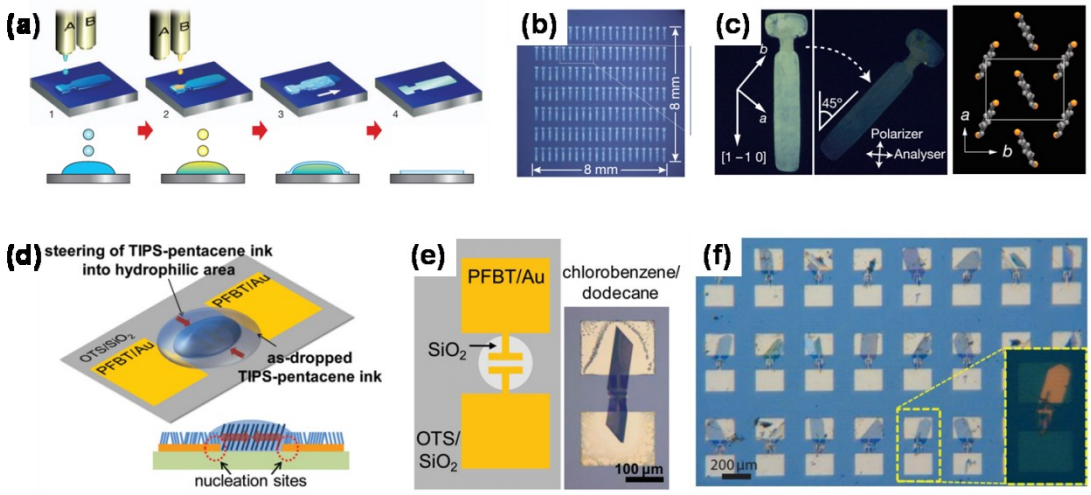

Figure 10. (a) Schematic illustration of the fabrication process of C_8-BTBT single crystals by using the combined method of inkjet-printing and antisolvent crystallization. (b) Image of a 20 × 7 array of the prepared C_8-BTBT single-crystals. (c) Cross-polarized micrographs of the C_8-BTBT single-crystal and its molecular arrangement in the crystal. (a-c) Reproduced with permission.[14] Copyright 2011, Nature Publishing Group. (d) Schematic illustration of steering TIPS-PEN ink into the hydrophilic area and the crystal growth of TIPS-PEN crystals. (e) As-prepared TIPS-PEN single-crystal spanning across Au electrodes on the patterned channel area. (f) An optical microscopy image of inkjet printed TIPS-PEN OFET arrays, the inset is a polarized optical microscope image of a single inkjet printed TIPS-PEN OFET. (d-f) Reproduced with permission.[119] Copyright 2012, Wiley.

Several groups have used inkjet-printing method to fabricate SMOSN arrays.[14,119] Minemawari, Hasegawa and co-workers demonstrated large area fabrication of C_8-BTBT single crystals by using combined methods of inkjet-printing and antisolvent crystallization.[14] Two miscible solvents with similar boiling points are selected as good solvent (1,2-dichlorobenzene, DCB) and poor solvent/antisolvent (N,N-dimethylformamide, DMF) for C_8-BTBT. A silicon substrate is pre-patterned with wetting and nonwetting areas by hexamethyldisilazane modification and ultraviolet/ozone treatment. The fabrication process is illustrated in **Figure**

10a. Poor solvent (DMF) was first printed at wetting areas, and then the solution of C_8-BTBT in good solvent (DCB) was deposited on the top of poor solvent (DMF), by using a piezoelectric inkjet-printing apparatus with double inkjet-printing heads. After that, they were left for slow evaporation, single crystal films of C_8-BTBT with thickness about 30-200 nm were obtained after solvent drying. Nucleation of C_8-BTBT molecules was observed to occur preferentially at the perimeters of the droplets (solid-liquid-air interfaces). These formed nuclei seeded the subsequent growth of crystals with the evaporation of the solvent. The authors found that the nucleation was very sensitive to the configuration of the droplets whose shape was dependent on depositing region and droplet volume. Thus they designed a depositing region with a protuberance. In this design, nucleation preferentially occurred at the protuberance due to its high surface area-to-volume ratio. After local seeding, the growing front moved to normal region, where growth of the crystals continued with solvent evaporation until a large uniform single crystal film was formed (Figure 10b,c). The successful deposition of such a uniform high quality single crystal film is attributed to the special shapes of the depositing regions in which crystallization and subsequent crystal growth can be separated. Depositing regions like a simple square, rectangle or circle can only produce polycrystalline films with some crystal domains. Other parameters such as the ratio between good and poor solvent, concentration of C_8-BTBT solution and substrate temperature are also crucial for effective deposition of single crystal film of C_8-BTBT. The printed C_8-BTBT crystals exhibited excellent transistor performance with average mobility as high as 16.4 $cm^2 V^{-1} s^{-1}$.

TIPS-PEN single crystal arrays were also inkjet-printed at electrode channel regions and high-performance devices were constructed as well.[119] In the process, a substrate was firstly pre-patterned with Au electrodes, and then modified with OTS to make a hydrophobic substrate surface. After that, it was treated with deep ultraviolet (DUV) irradiation through a patterned quartz mask, wettability of the exposed channel area was considerably enhanced from hydrophobic into hydrophilic. Then TIPS-PEN in a co-solvent system of

chlorobenzene/dodecane mixture with 3:1 volume ratio was inkjet-printed on the substrate, as illustrated in Figure 10d. The ink flowed towards the electrode channel area due to surface energy difference between the hydrophilic channels and hydrophobic surrounding areas. With solvent evaporation, Marangoni flow against coffee-ring effect directed the formation of homogeneous crystals at controlled channel regions.[120] TIPS-PEN single crystal arrays were finally formed, spanning across Au electrodes (Figure 10e). OFET device arrays were constructed accordingly (Figure 10f). Surface wettability property plays a key role in the formation of large uniform single crystals. Hydrophobic OTS/SiO_2 surface (contact angle of 90°-110°) will induce small diameter of dropped ink without pinning effect during solvent evaporation and thus non-crystallized structures are produced. In comparision, a less hydrophobic surface (contact angle of 60°-70°) allows the solvent to be pinned at the edge of the droplet and thus easily leads to the formation of multiple crystals driven by the coffee-ring effect.

2.3.2. Transfer-printing

Transfer-printing often involves the fabrication of NWs at a donor substrate followed by being transferred to a receiver substrate to form highly aligned arrays through surface chemical or physical interactions.[121] The dominant physical/chemical interactions usually involve capillary force and van der Waals interactions. Contact-printing is one special kind of the transfer-printing methods, which involves the fabrication of randomly aligned NWs at a donor substrate and the transfer of NWs to a receiver substrate to obtain highly aligned arrays by applying directional shear force.[122] During this process, the detachment and alignment of randomly oriented NWs from the growth substrate are achieved through the directional shear force. The anchor of aligned NWs on the receiver substrate is realized through van der Waals interactions between NWs and the substrate. Contact-printing is a general method to create aligned NWs. It is particularly effective for the transfer and alignment of NWs on flexible substrates.[123-127] In another type of transfer-printing method, highly aligned NWs are firstly formed using a

template method, and then capillary force is utilized to pull the NW arrays down from growth template to a receiver substrate.[36,128,129]

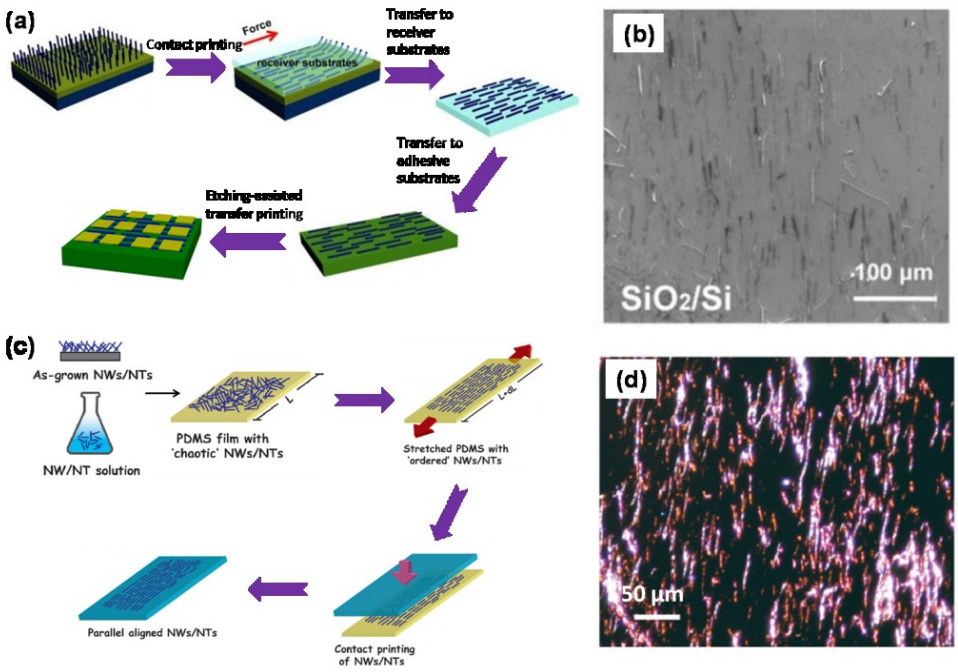

Figure 11. (a) Schematic illustration of the two-step transfer-printing method for the fabrication of NW array based devices. (b) SEM image of the transferred NW array on SiO_2/Si substrate. (a,b) Reproduced with permission.[130] Copyright 2014, Nature Publishing Group. (c) Schematic illustration of the stretched contact-printing method for assembly of randomly dispersed NWs from solution into aligned arrays. (d) Dark field optical image of organic NW arrays transferred from a randomly dispersed solution. (c,d) Reproduced with permission.[131] Copyright 2012, American Chemical Society.

Deng, Zhang and co-workers have demonstrated a two-step transfer-printing method to achieve various organic NW array-based devices including resistors, diodes and top-gate OFETs on diverse conventional or curved and non-planar substrates which are not accessible before.[130] The transfer-printing process is illustrated in **Figure 11**a. Copper phthalocyanine (CuPc) NWs were synthesized by physical vapor deposition method on the growth substrate with random orientations. Then the NWs were transfer-printed on receiver substrates like

SiO_2/Si and glass by applying directional shear force, resulting in highly aligned arrays with controllable density (Figure 11b). Such NWs can be further passed to an adhesive substrate like PDMS and tapes. Following this, electrodes can be further transferred to these adhesive or nonadhesive substrates bearing with NW arrays via an etching-assisted transfer-printing method.[130] Finally, a variety of devices can be constructed, which were observed to exhibit similar or even better performance than those devices fabricated from conventional methods.

A stretched contact-printing method was recently proposed to assemble random dispersed NWs from solution or vapor phase into aligned arrays.[131] As illustrated in Figure 11c, NWs were fabricated at first by solution or vapor deposition method. Then they were randomly dispersed on the stretchable PDMS substrate, which was subsequently held with home-designed two foldback clips and stretched to different distance at a controlled speed. The stretch would induce disordered NWs to gradually transform into ordered and highly aligned arrays. After that, contact-printing process was performed to release the ordered NWs from PDMS to any desirable substrate (e.g., rigid SiO_2/Si and flexible substrates), forming a monolayer of oriented NW arrays on the surface (Figure 11d). The authors also demonstrated that this method was applicable to various types of materials including organic NWs, inorganic NWs and carbon nanotubes either from solution dispersions or as-grown substrates. Different devices based on the as-transferred NW arrays were fabricated, including aligned multi-silicon NWs-based OFETs and hybrid inorganic-organic OFETs. All these results demonstrated the feasibility of making NW array-based devices using this stretched contact-printing method.

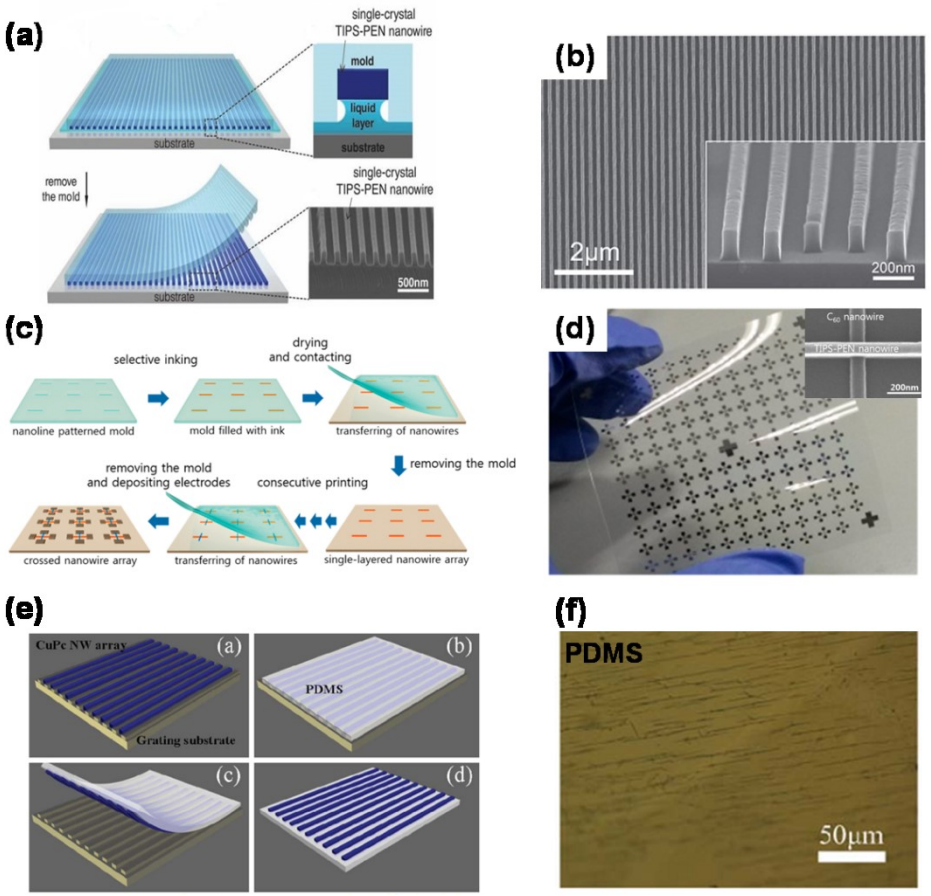

Figure 12. (a) Schematic illustration of the liquid-bridge-mediated nanotransfer molding method. (b) SEM image of TIPS-PEN NW arrays fabricated on a Si substrate. Inset is corresponding perspective magnified view of the NW arrays. (a,b) Reproduced with permission.[36] Copyright 2013, Wiley. (c) Schematic illustration of the fabrication process of cross-stacked organic p-n nanojunction arrays. (d) Photograph of organic NW p-n nanojunction arrays on a PES substrate, the inset is SEM image of cross-stacked single-crystalline TIPS-PEN/C_{60} NWs. (c,d) Reproduced with permission.[132] Copyright 2014, American Chemical Society. (e) Schematic illustration of the transfer process of CuPc NW arrays from the grating substrate to the plastic substrate. (f) Optical image of the transferred CuPc NW arrays on PDMS substrate. (e,f) Reproduced with permission.[134] Copyright 2012, The Royal Society of Chemistry.

Another kind of transfer-printing method named "liquid-bridge-mediated nanotransfer molding method" was proposed by Park *et al*. In this method, organic NWs are fabricated within nanochannels and then transfer-printed to a target substrate.[36] The brief transfer mechanism is presented at **Figure 12**a. Single-crystalline organic NW arrays (TIPS-PEN) were formed via self-assembly method from solutions within nanoscale channels on a pre-patterned polyurethane acrylate (PUA) template. Then the template was placed on a substrate surface covering with some polar liquid as a lubricant layer. A capillary bridge was formed between the NWs and substrate. With evaporation of the polar liquid, increased capillary force would draw NWs down from PUA template to the substrate. Thus the NW arrays formed at PUA template were successfully transfer-printed to the receiver substrate (Figure 12b). By using this method, the authors also fabricated aligned NW arrays of fullerene (C_{60}), poly(3-hexylthiophene) (P3HT) and indolocarbazole derivatives at specific positions. More complex NW array structures such as two-layer crossed-stacked TIPS-PEN NW arrays were also fabricated by repeating the transfer-printing process on a substrate. Recently, cross-stacked organic p-n junction nanoarrays made of single-crystal TIPS-PEN and C_{60} NWs as p-type and n-type semiconductors respectively, were also fabricated by using the transfer-printing method.[132] The fabrication process is displayed in Figure 12c. C_{60} NWs were fabricated within PUA nanochannels and then transfer-printed to a receiver substrate at desired locations. Then TIPS-PEN NWs were placed as the second layer using the same method. A polar solvent that cannot dissolve TIPS-PEN and C_{60} NWs was used as the liquid-bridge to make good conformal contact between PUA template containing TIPS-PEN NWs and the substrate bearing with pre-patterned C_{60} NWs. With solvent evaporation, TIPS-PEN NWs were sucked down by strong capillary force, leading to the formation of a crossed p-n junction array of single-crystal organic NWs. The authors showed that p-n junction arrays of single-crystal TIPS-PEN/C_{60} NWs could be fabricated on a 8 × 8 cm^2 poly(ethersulfone) (PES) substrate (Figure 12d). After silver electrodes were deposited on each end of NWs, single-crystal organic NWs p-n junction array

based devices were then constructed. These devices demonstrated good rectifying behavior and photodiode characteristics. Besides PUA, pre-patterned PDMS with periodic lines can also serve as the growth template for aligned growth of organic NWs.[133] In another example, a PUA grating substrate (1600 lines) serves as the template for oriented growth of CuPc NWs in vapor phase, and then PDMS is utilized as an elastic stamp and receiver substrate for the transfer of NW arrays.[134] The process is shown in Figure 12e. After aligned growth of CuPc NWs on the PUA template, liquid PDMS was cast onto the grating substrate containing of NW arrays and kept for 1 h, and then followed by curing at 50 °C for 12 h. Once the PDMS was peeled off, aligned CuPc NW arrays were successfully transfer-printed onto the flexible PDMS substrate (Figure 12f). Photodetectors were constructed on the transparent and mechanically flexible PDMS substrate, which demonstrated pronounced photoresponse to incident light.

Oh and co-workers also reported an excellent transfer method, named filtration-and-transfer (FAT) method, for alignment of SMOSN with controllable density as well as the formation of multiple patterns in differnt directions.[135] In this method, organic NWs were fabricated by a solution method, and then filtered through a PDMS mask patterned porous anodized aluminum oxide (AAO) membrane under vacuum. After filtration, NWs were deposited out and formed aligned patterns. The density of aligned NWs can be easily tuned by varying the concentration of NW dispersion. By placing the AAO memberane carrying with aligned NW patterns to a SiO_2 wafer with a hydrophobic surface, NW patterns can be readily transferred from the hydrophilic AAO memberane to the target substrate. This technique allows for the formation of multiple NW patterns aligned in different directions on the same substrate, and it is also applicable to flexible substrates.

2.3.3. Template-induced printing

Template-induced printing method usually employs a template to assist the printing of aligned patterns on a substrate.[136] Elastomeric PDMS with periodic lines (or shapes) is mainly used as the template.[137] A variety of techniques have been demonstrated to use PDMS as the template

to induce printing of nanopatterns, which can be divided into two types.[23,24,61-71,138,139] One type makes use of template-induced self-assembly process to print aligned patterns on a substrate, which has been elaborated in the "template-induced self-assembly" section. The other type is to grow a crystalline film on a substrate and then the film is imprinted by a PDMS template into desired array patterns.

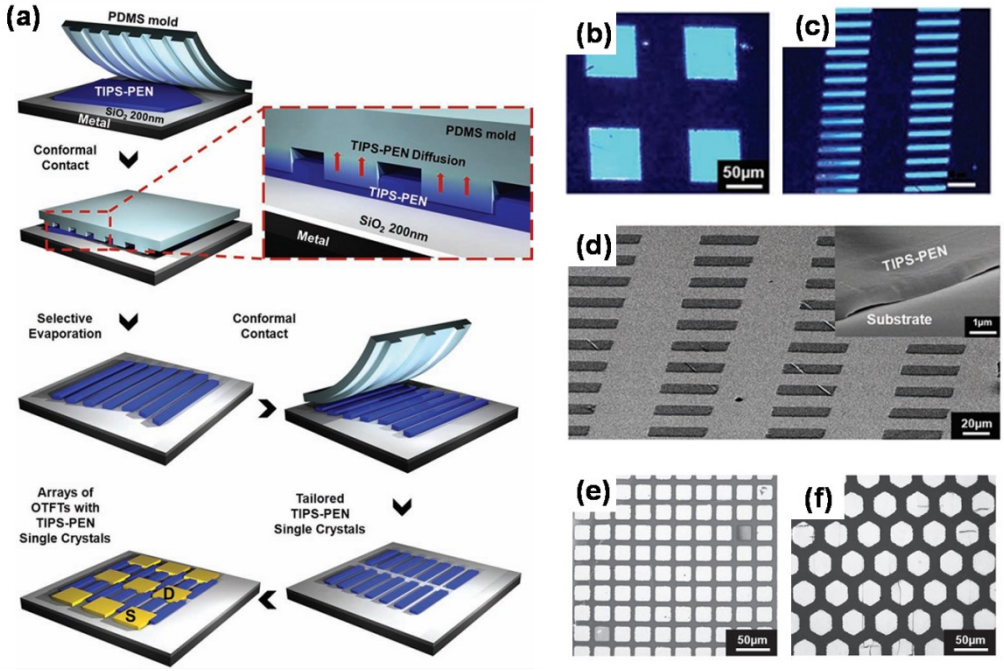

Figure 13. (a) Schematic illustration of the selective contact evaporation printing process. (b) and (c) are optical microscopy images of micropattens of TIPS-PEN single crystal with various shapes and sizes. (d) SEM image of the rectangular TIPS-PEN single crystal patterns, inset is the magnified image showing the smooth edge. (e) Square holes arrayed in *p4mm* symmetry and (f) hexagons arrayed in *p6mm* symmetry fabricated by selective contact evaporation printing. (a-f) Reproduced with permission.[138] Copyright 2011, Wiley.

A so-called selective contact evaporation printing method was reported, as depicted in **Figure 13**a.[138] TIPS-PEN was first dissolved in mixed solvent of 50/50 (wt%/wt%) dodecane/toluene. The solution was then drop-cast on a substrate for controlled evaporation to make a flat and uniform crystalline film. Subsequently, a PDMS mold with periodic lines was

pressed on the substrate with proper pressure (3 kPa) followed by heat treatment at 100 °C for 1 h. Next, TIPS-PEN was selectively evaporated at the regions in contact with the topographic PDMS template and molecules diffused into PDMS template. After removal of PDMS template, well-defined single-crystalline TIPS-PEN NW arrays were printed on the substrate. By using two PDMS templates with periodic lines of different width and periodicity for selective etching of TIPS-PEN on the substrate, square and rectangular microdomains with dimensions of 50 × 50, 25 × 25, 10 × 10, 100 × 20, 75 × 10, and 50 × 20 μm^2 were successfully fabricated (Figure 13b-d). Patterns with various shapes arrayed in different symmetries including square holes and hexagons, could also be easily achieved by changing shapes of PDMS templates (Figure 13e,f). It was found that two key factors played crucial roles for selective etching of TIPS-PEN film. One is the good conformal contact between the template and TIPS-PEN surface on the substrate, which ensures effective heat accumulation at the contact areas to drive solution diffusion into PDMS. Another is to have sufficient free volume in the elastomeric PDMS template, which permits efficient inward diffusion of TIPS-PEN molecules. Based on the as-prepared micropatterns of TIPS-PEN crystals, bottom gate OFETs were fabricated, with mobility of approximately 0.36 $cm^2 V^{-1} s^{-1}$ and an on/off current ratio of 10^6.

Compared with other printing methods, template-induced printing method has several advantages: i) easy to control crystal diameter by tuning corresponding template channel sizes; ii) diverse pattern shapes can be achieved through template design; iii) low-cost and highly effective. However, there are also several concerns: i) it is difficult to fabricate PDMS templates with nanoscale patterns although they are more useful in future highly integrated devices; ii) the template detachment process often causes inevitable damages to crystals.

3. Vapor-processed techniques for alignment and patterning of SMOSN

3.1. Physical vapor deposition

Physical vapor deposition (PVD) method has been extensively used for the fabrication of SMOSN. In a typical process, source materials are heated above their sublimation temperature

(T_s) under vacuum, and then they are transported to a low-temperature zone by gas flow, where molecules deposit out and grow into nanocrystals.[140,141] Since no solvent or impurities are involved in PVD process, the resulting SMOSN normally have excellent crystal quality with limited disorder, which is much better than those grown from solution-processed methods. However, PVD methods usually suffer from problems like low yield/output for large-scale device applications and high-temperature processes.[40,142-145] Particularly, it is relatively difficult to precisely control alignment and patterning of SMOSN in PVD processes, in contrast to solution-processed methods. Therefore, only several techniques have been reported so far.[48,146-153]

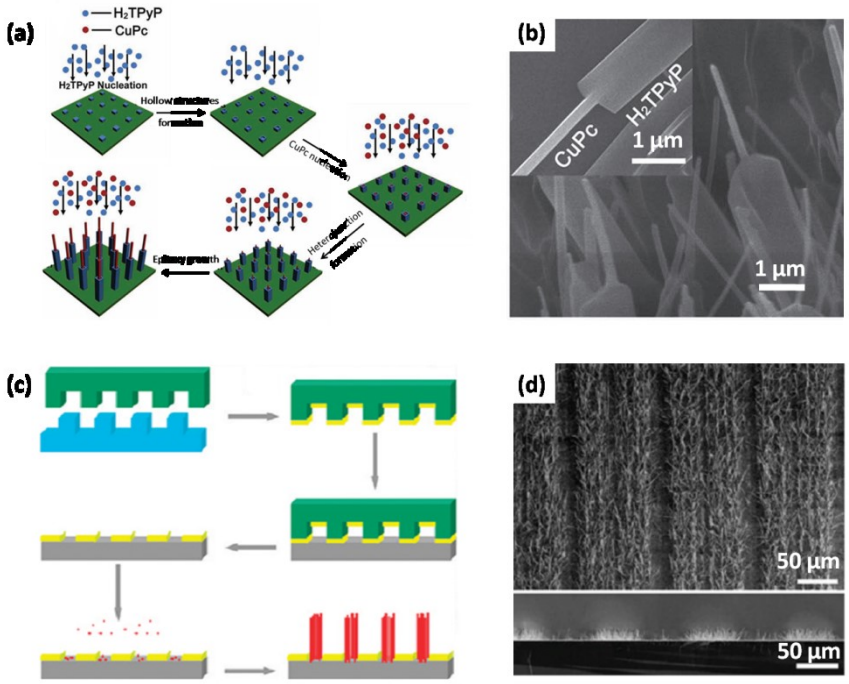

Figure 14. (a) Schematic illustration of the growth process of the coaxial organic p-n heterojunction NW arrays of CuPc/H_2TPyP. (b) SEM image of the p-n junction NW arrays. Inset is a SEM image of a single junction wire. (a,b) Reproduced with permission.[48] Copyright 2012, Wiley. (c) Schematic illustration for the PDMS patterned growth of vertically aligned DAAQ NW arrays. (d) The 40° tilt view and cross sectional view SEM images of vertically aligned DAAQ NWs. (c,d) Reproduced with permission.[147] Copyright 2010, American Chemical Society.

Vertically aligned organic NWs of 1,5-diaminoanthraquinone (DAAQ) were prepared on various solid surfaces (e.g., Si, glass, Au, Al, Fe and Cu foils) by employing PVD method.[146] In the fabrication, a DAAQ film is homogeneously coated on the inner wall of a round bottle flask. Then the flask was heated to the temperature of sublimation (150-200 °C) to vaporize the powders. With DAAQ vapor transferred downstream to a receiver substrate at low temperature region by gas flow, DAAQ NW arrays grew vertically on the substrate. It was observed that vertically oriented DAAQ NPs with diameters of about 100 nm were grown on the substrate at early stage, and then they served as the seeds for the subsequent oriented growth of DAAQ NWs. With this technique, coaxial organic p-n heterojunction NW arrays of CuPc (p-type) and 5,10,15,20-tetra(4-pyridyl)-porphyrin (H_2TPyP, n-type) were fabricated.[48] The growth process is shown in **Figure 14**a. CuPc and H_2TpyP powders in individual boats were put at different temperature zones to make a co-evaporation system. H_2TPyP at a higher temperature zone with faster evaporation rate was first deposited on the substrate, forming vertically aligned H_2TPyP NPs. Then hollow structures appeared on the top of NPs, and served as higher energy areas for the subsequent selective nucleation of CuPc. Subsequently, the two materials grew separately and gradually formed vertically aligned core/shell heterostructure arrays (Figure 14b). The intimate connection at the junctions endows the ordered arrays of organic p-n heterojunctions with a great potential of applications in excellent organic optoelectronic devices.[48]

Molecules are observed to preferentially nucleate and grow much faster at high surface energy sites such as dust particles and scratches.[147,148] Keeping this in mind, Zhao *et al*. pre-patterned a substrate with a self-assembled monolayer to offer different surface energy areas and achieved patterned growth of vertically aligned SMOSN.[147] The patterning process is briefly illustrated in Figure 14c. First, a substrate was treated to be hydrophilic, and then a PDMS stamp with periodic lines was inked with (tridecafluoro-1,1,2,2-tetrahydrooctyl)triethoxysilane (FOTES), and printed directly onto the substrate. The

unstamped areas with hydrophilic properties become the higher surface energy domains. When PVD method was used, ordered NW arrays were selectively patterned on the hydrophilic areas (Figure 14d).

3.2. Guided physical vapor deposition (GPVD)

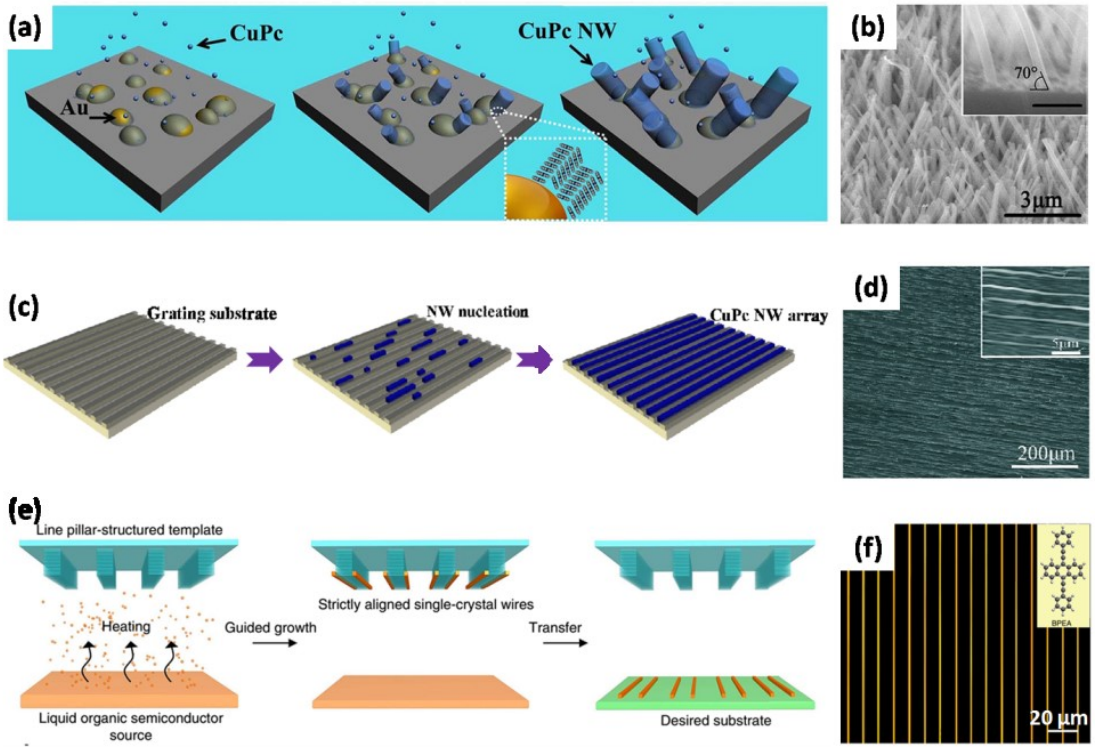

Figure 15. (a) Schematic illustration of growing the cross-aligned CuPc NW arrays on Au-film coated substrates. (b) SEM image of the cross-aligned CuPc NW arrays, inset is a magnified SEM image of the NW arrays with alignment angle of 70°. (a,b) Reproduced with permission.[50] Copyright 2013, Nature Publishing Group. (c) Schematic illustration shows the growth process of the template-guided method by grating grooves. (d) SEM image of aligned CuPc NW arrays grown on the grating substrates. Inset is the high magnification image of CuPc NWs. (c,d) Reproduced with permission.[134] Copyright 2012, The Royal Society of Chemistry. (e) Schematic illustration of the process of using the pillar-structured substrate as the template to guide the PVD process to fabricate aligned and patterned BPEA NW arrays. (f) A dark-field fluorescent micrograph of BPEA NW arrays on a flat PDMS film. Inset is the molecular

structure of BPEA. (e,f) Reproduced with permission.[22] Copyright 2015, Nature Publishing Group.

Another route to pattern SMOSN in PVD process is to use metallic NPs as active sites to guide patterned growth of nanostructures.[50,149-153] It has been discovered that Au NPs can serve as the nucleation sites and direct anisotropic growth of planar phthalocyanine derivatives for 1D nanostructure with precise localization and tunable dimensions.[149,150] Wu, Jie and co-workers demonstrated large-area fabrication of cross-aligned CuPc NW arrays on Au-film coated substrates.[50,152] The schematic illustration of this method is shown in **Figure 15**a, a layer of Au film (thickness ~50 nm) was coated on a substrate followed by a PVD process. It was found that growth of NW arrays started from Au NPs, and the formed NWs were straight with crossed alignment (average alignment angle ~70°) (Figure 15b). With utilization of photolithography technique to control the location of Au NPs-coated areas, it was feasible to achieve precisely patterned growth of CuPc NW arrays at desired locations. Various patterns including parallel, grid-like and even some complex structures were fabricated by tuning the geometries of Au-coated areas. Besides Au film, silver (Ag) film can also direct aligned growth of CuPc NW arrays. This technique also allows for patterned growth of NW arrays of other organic semiconductors, such as 3,4,9,10-perylenetetracarboxylic dianhydride (PTCDA). By pre-patterned Au electrodes on a substrate, NW array patterning and device integration can be achieved simultaneously. Such integrated devices exhibited high yield, high integration level, small pixel-to-pixel variation, and could function as a high-resolution image sensor.[153]

NW arrays produced by pure PVD process and metallic NPs guided process are predominantly vertically aligned. However, for practical device applications, it is more desirable to have NW arrays with in-plane alignment on the substrates.[22,134] Recently, other mechanisms based on template-guided PVD processes have been developed. As one example, grating grooves have been reported to act as an alignment template to guide oriented growth of

in-plane CuPc NW arrays.[134] As described in Figure 15c, a PUA grating substrate (~1600 lines) fabricated by nanoimprint was adopted as a receiver substrate. After PVD process, highly ordered CuPc NW arrays along the grating grooves were obtained on the flexible PUA substrate (Figure 15d).[134] It was proposed that vaporized CuPc molecules were absorbed in the grating trenches and formed nuclei, then lateral coming molecules would continue growing on them and slowly fused together to form NWs along the grating trenches. The growth orientation of NWs is navigated by the underlying topographical patterns of the template. The NW arrays can be easily transferred to other desirable substrates for device applications by using PDMS as elastic stamp.

Recently, a method of using a pillar-structured substrate as the template to guide PVD process has been reported for controlled alignment and patterning of 9,10-bis(phenylethynyl)anthracene (BPEA) NW arrays.[22] The process is illustrated in Figure 15e, a BPEA/ethanol solution in a metal boat served as the evaporation source. A pillar-structured silicon substrate with surface microstructures including parallel lines, squares, hexagons or 'X' structures was used as a receiver substrate and placed facedown onto the metal boat. Next, the boat with the solution was heated to 180° C in air (near the sublimation temperature of BPEA) for solvent evaporation and material deposition. Due to the surface energy difference between the pillar tops and sidewalls, BPEA was observed to preferentially nucleate at the pillar edges. These nuclei kept growing until joining together along the orientation of the pillar edges, resulting in highly aligned NW arrays. Unlike many other reported PVD methods, the fabrication process can be performed in air or nitrogen environment, but no NWs were able to be produced under vacuum conditions. Besides parallelly aligned NW arrays, various patterns of jointed NWs with precisely controlled internal angles were fabricated by adjusting pillar geometries. NW arrays can be easily transferred onto other desired substrates by a simple contact-printing method. By using the patterned NWs with tunable internal angles, various optical waveguides have been demonstrated.

4. Device applications of the aligned/patterned SMOSN

In the above sections, we have extensively reviewed a broad range of solution and vapor processed techniques for precise alligning and patterning of SMOSN. These technologies build up the foundation of the applications of SMOSN in a diversity of devices. Accordingly, we will next highlight the classical advancement of SMONS devices including photodetectors, imaging sensors, OFETs and logical circuits.

4.1. Photodetetors and image sensors

Photodetector is a type of optoelectronic device that can transform optical signals to electrical signals, and has important applications in diverse fields, such as imaging, optical communication, security, and defense.[154-158] In general, the photodetectors can be divided into three types, including photoconductors, photodiodes, and phototransistors.[159-169] Photoconductors have the simplest device structure, in which a semiconductor is sandwiched between two ohmic-contacted metal electrodes. Photodiodes are two-terminal devices too, but p-n junctions or Schottky junctions are usually introduced to enhance the built-in electric field for photocarriers separation and transportation. Phototransistors are three-terminal devices and basically have the same configuration as OFETs. For these devices, an additional gate electrode offers the ability to modulate the photoresponse of devices by an electric field in the gate region. Generally, the key figure-of-merit parameters of responsivity (R), photoconductive gain (G), detectivity (D^*), and response speed are used to evaluate the performance of a photodetector. However, for an image sensor, which consists of many photodetectors in a circuitry to achieve imaging functionality, other parameters such as yield, integration density, and reproducibility of the pixels are equally important.

Single-crystalline SMOSN constitute a promising platform to study the intrinsic photoconductive characteristics of organic crystals.[170-175] For instance, photoconductors based on benzothiophene nanoribbons exhibited a high photoconductivity gain of 1.3×10^4 and a high responsivity of 4372 A W^{-1} at 405 nm.[170] Phototransistor based on microplates of anthracene-

based materials was also used as a photodetector, a high photoresponsivity of >1 × 10^4 A W^{-1} and an on/off current ratio of >10^3-10^5 was obtained.[175] The overall performance of these SMOSN-based photodetectors is comparable to some inorganic nanostructure based ones. Recent development in fabrication of large-scale aligned/patterned SMOSN has stimulated the studies on SMOSN array-based photodetectors. Zhang and coworkers developed a grating-assisted PVD method for large-scale growth of aligned ultralong CuPc NWs on a PUA grating substrate,[134] enabling the fabrication of transparent and flexible photoconductors based on organic NW arrays. Response of the device to the pulsed light was fast, highly stable, and reproducible. Additionally, the performance remained unchanged after bending to a curvature of 0.5 cm^{-1}. The NW arrays could be further transferred from the grating substrate to a PDMS stamp, and the resultant photoconductors displayed excellent flexibility and stretchability. Phototransistors were demonstrated based on TCNQ microcrystal arrays, which were grown via a local growth in solution with the assistance of a glass capillary tube.[176] These phototransistors with polymeric gate dielectric exhibited stable n-type characteristics with a low threshold voltage of < 0.5 V. Under light illumination, the devices produced a current on/off ratio of 31 at a gate voltage of 0.3 V. Though the device exhibited a moderate responsivity of 1 mA W^{-1}, its response speed was fast (10 ms). Large-scale fabrication of organic NW phototransistors in the bottom gate, top contact transistor configuration was reported by Park *et al*.[36] By tuning the gate voltage, the flexible phototransistors displayed a maximum current on/off ratio of 10^3 at a gate voltage of 4 V, along with a high responsivity of 3.5 × 10^3 A W^{-1}, under white light illumination (12.2 mW cm^{-2}).

Owing to the large-area uniformity, high sensitivity, and broadband response, SMOSN arrays are promising building blocks for high-performance image sensors. Compared to conventional silicon-based charge coupled device (CCD), SMOSN array-based image sensors have unique advantages in terms of light weight, high flexibility and low cost etc.[177] However, high-density integration of SMOSN array-based photodetectors remains a bottle neck for their

practical applications. Zhang *et al*. developed an in-situ integration technique to achieve large-scale integration of SQ NW array-based photodiodes by growing NW arrays on pre-patterned electrodes through an evaporation-induced self-assembly process.[26] Asymmetric electrode pairs of Au-Ti were utilized for the construction of Schottky-type photodiodes based on NW arrays. These devices exhibited high current on/off ratio, fast response, and low-light detection capability of each pixel in the integrated photodetector circuitry. Due to the homogeneously assembled NW arrays, the photodiodes disclosed a high uniformity with a mean rectification ratio of around 1200-1500 in the dark. Most pixels had almost the same sensitivity with a very small pixel-to-pixel variation. High yield of the operational pixels with a high level of integration makes this assembly strategy very useful for the future image sensor applications. Very recently, a really functional image sensor was demonstrated by Wu, Jie and coworkers. Cross-aligned CuPc NW arrays were directly grown on pre-fabricated electrode circuit via a PVD method (**Figure 16**a-f).[50] The relative low growth temperature (~180 ^{o}C) of CuPc NW arrays makes this in-situ growth possible. A unique read-bus structure was adopted for the sensor circuitry, ensuring high integration level of the devices. The integrated image sensor contained a 10 × 10 pixel array in an area of 1.3 × 1.3 mm^2. Surface area for each pixel (130 × 130 μm^2) was smaller than the pixel size (800 × 800 μm^2) in previous reports for inorganic image sensors that have discrete device structure.[178,179] Due to high uniformity of NW arrays, near 100% of the pixels could successfully operate at a high response speed and relatively small pixel-to-pixel variation. The yield of this image sensor also surpassed those of image sensors fabricated from parallel-aligned inorganic NW arrays in previous studies, in which the yields were generally lower than 80%.[178,179] By projecting a red laser beam with a point diameter of 1 mm onto the corner of the sensor circuitry (Figure 16e,f), it was demonstrated that the circuit matrix of the organic photodetector could function as a high-resolution image sensor.

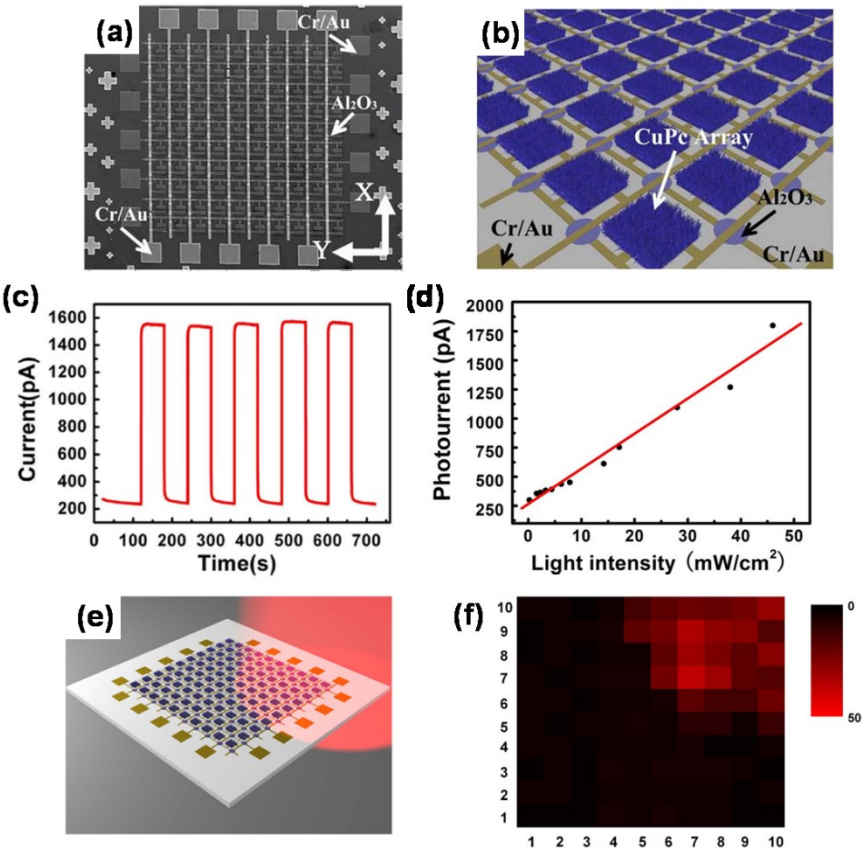

Figure 16. (a) SEM image of the as-fabricated integrated image sensor, which contains a 10 × 10 pixel array in an area of 1.3 × 1.3 mm^2. (b) Schematic illustration of the image sensor circuit based on cross-aligned CuPc NW arrays. (c) Photo-response measurements of the pixel under pulsed light illumination. (d) Light intensity-dependent photocurrent of the image sensor. (e) Schematic illustration of the measurement configuration for demonstrating the feasibility of the sensor for spatial imaging. A red laser beam was projected onto the right-upper corner of the sensor circuitry. (f) The corresponding 2D intensity distribution of (e) measured by mapping the pixel signals, matching the shape of the laser beam. Reproduced with permission.[50] Copyright 2013, Nature Publishing Group.

In spite of the rapid progress, it is noteworthy that study on SMOSN-based photodetectors still remains at an early stage. Performance of SMOSN-based photodetectors needs to be further enhanced. For instance, most of SMOSN-based photodetectors have a response speed in the range of 10 ms ~1 s,[160] presumably due to the relatively low carrier mobility of organic

material, long transit time of lateral structure photodetectors, and existence of surface defects/traps. This response speed is still too low to fulfill the demand of practical applications such as optical communication and high-speed imaging. Growth procedures as well as device structures of SMOSN should be further optimized to improve the response speed. In addition, it remains a challenge to fabricate integrated photodetectors based on SMOSN arrays due to the incompatibility of organic crystals with conventional microfabrication techniques such as photolithography and sputtering. Consequently, it is essential to establish more efficient methods to improve the integration level for high-resolution image sensor applications. There is a large room for exploring the applications of SMOSN in flexible and stretchable photodetectors, which may bring new opportunities for their practical applications.

4.2. OFETs and logic circuits

OFETs are fundamental elements of organic electronics, and they have found many potential applications in a variety of fields, such as active matrix displays,[180,181] electronic paper,[182,183] sensors,[103,184,185] and radio-frequency identification cards.[186,187] OFETs are three-terminal devices. Besides organic semiconductor that acts as device channel, other basic device components include source and drain electrodes, gate electrode, and gate dielectric layer. Source-drain current that flows through organic conduction channel can be modulated by an external electric field applied on the gate electrode, allowing switching of the device between on and off states. Various parameters such as field-effect mobility, on/off current ratio, and threshold voltage are commonly adopted to characterize the performance of OFETs. The performance of OFETs strongly depends on electronic properties of organic semiconductors. Compared with their thin film counterpart, SMOSN possess superior electronic properties due to higher crystal quality and fewer grain bounderies/defects, which enables the construction of SMOSN-based OFETs with remarkably higher performance.[6-8] With the development in patterning/alignment techqiues for SMOSN, SMOSN-array based OFETs have achieved big progress. In this section, we will discuss the OFET applications of SMOSN. The development

of single SMOSN-based OFETs will be briefly summarized at first, and then emphasis will be placed on the OFET applications of patterned/aligned SMOSN arrays.

It is impressive that field-effect mobilities of SMOSN have experienced a rapid increase in the past few years, through the optimization on molecular structures, growth conditions, and device structures of OFETs.[188-191] P-type SMOSN with hole mobility around 10 $cm^2 V^{-1} s^{-1}$, which is much higher than that of amorphous silicon (~1 $cm^2 V^{-1} s^{-1}$), have been reported by many groups.[15,191-193] For example, it was reported C_8-BTBT microcrystals fabricated from solvent vapor annealing method possessed a mobility of 9.1 $cm^2 V^{-1} s^{-1}$.[192] Recently, microribbon-shaped β-phase dihexyl-substituted DBTDT (C_6-DBTDT) crystals fabricated from solution phase were reported to exhibit a hole mobility up to 18.9 $cm^2 V^{-1} s^{-1}$.[15] Compared with p-channel OFETs, n-channel SMOSN-based OFETs are less developed, and investigation on n-channel OFETs usually reveals a lower electron mobility of 1~5 $cm^2 V^{-1} s^{-1}$, due to the lack of air stable n-type organic semiconductors.[194-196] It has been revealed that significant π-orbital overlap between neighboring molecules can greatly facilitate charge carrier transport and enable high mobility.[1,197] As such, He and coworkers took advantage of close molecular packing of 2,6-Dichloro-1,4,5,8-naphthalene tetracarboxylic dimide (Cl_2-NDI) molecules, and fabricated air stable Cl_2-NDI microribbon based n-type OFETs with electron mobility up to 8.6 $cm^2 V^{-1} s^{-1}$ and on/off current ratio of 7×10^7.[198]

SMOSN-array based OFETs have now gained great progress, owing to the emerging successful alignment/patterning techniques and the corresponding device fabrication strategies for SMOSN. Device fabrication methods like shadow mask,[64,73] inkjet-printing,[94] in-situ device integration,[33,77,119,199] and transfer-printing [29,197,200] have been developed for

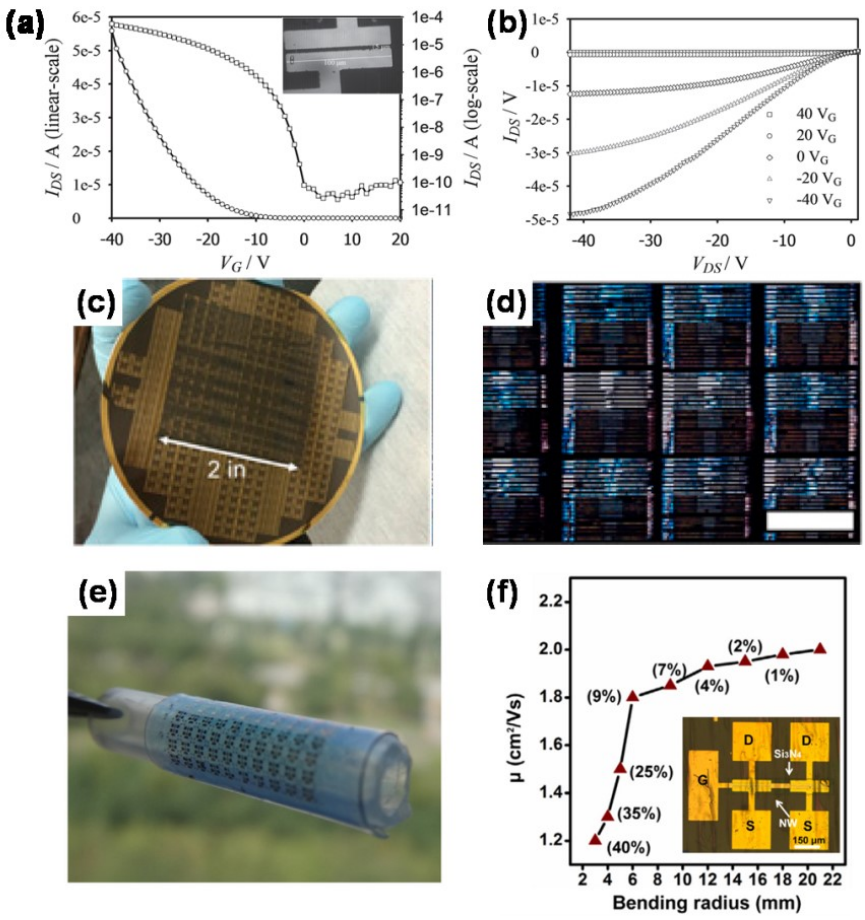

Figure 17. (a) Transfer curve and b) output curve of the aligned TIPS-PEN based OFET. Inset in (a) was an optical image of device. (a,b) Reproduced with permission.[73] Copyright 2014, Wiley. (c) Image of electrodes patterned on a 4-in wafer with blade-coated TIPS-PEN. (d) Cross-polarized optical image of transistors of a section on the wafer shown in (c). The scale bar is 3000 μm.) (c,d) Reproduced with permission.[199] Copyright 2015, National Academy of Sciences of the United States of America. (e) Image of the flexible CuPc NW based OFET arrays with bending radius of 3 mm. (f) Mobility of the flexible OFET as a function of bending radius. Inset shows the optical image of a typical CuPc NW based OFET. (e,f) Reproduced with permission.[200] Copyright 2014, Elsevier.

the construction of OFET device arrays (**Table 1**). As a simple method, shadow mask method has been widely adopted for organic electronics.[14,64,73] This method involves direct deposition of metallic electrodes through a shadow mask that constitutes a stainless steel/plastic sheet with

open windows or small-diameter metal wires, thus avoiding direct photolithography on organic semiconductors. Since electrode evaporation is usually performed in high vacuum, this method is favourable for obtaining a good electrode/semiconductor contact for high-performance OFETs.[4,73] For example, Bao and coworkers prepared aligned crystalline domains of TIPS-PEN and then parylene shadow mask were placed on top of the substrates for thermally evaporating of Au electrodes as source and drain. The constructed OFETs yielded a high mobility of 2.7 cm^2 V^{-1} s^{-1} (**Figure 17**a,b).[73] However, in shadow mask method, size of the device is usually restricted by the feature size of the mask, which depends on the manufacturing techniques and normally is much larger than that produced by photolithography. To reduce the feature size of shadow mask for sophisticated device fabrication, a possible way is to fabricate free-standing polymer mask from polystyrene (PS), PMMA, and PUA and so on by photolithography.[45,201] This approach offers the possibility to fabricate OFETs with similar accuracy as that of photolithography.

Inkjet-printing method offers an effective approach to fabricate OFET arrays based on SMOSN.[94] Liu and coworkers presented an all-solution processing method to fabricate OFET arrays.[94] In the method, aligned organic NW arrays were patterned via dip-coating method, and then source-drain electrodes were fabricated by inkjet-printing conducting polymer PEDOT:PSS. Size of organic NW transistor arrays was determined by the density of printed electrodes, and 750 independent transistors were formed at 2 mm × 3.5 mm area. The devices in arrays showed an average hole mobility of 0.51 cm^2 V^{-1} s^{-1}. Despite the high efficiency, in inkjet-printing method, the registration capability of instrument restricted the alignment accuracy, whereas the attainable droplet size limited the size of each OFET.

Table 1. OFET device data for aligned/patterned SMOSN.

SMOSN	μ [$cm^2V^{-1}s^{-1}$]	I_{on}/I_{off}	V_{Th} [V]	Alignment/Patterning Method	Device Fabrication	Device Architectures[a)]	Ref.
C_8-BTBT	31.3	10^5-10^7	-10	inkjet printing	shadow mask	TGTC; Au; parylene C	[14]
C_8-BTBT	3.5	10^7	-0.6	spin-coating	shadow mask	BGTC; Au/MoO_X; Si/SiO_2; tested in air	[76]

C_8-BTBT	2.6	10^5		template-guided self-assembly	shadow mask	BGTC; Au; Si/SiO_2; tested in air	[63]
C_8-BTBT	0.53	10^9	-0.062	wettability-guided self-assembly	in-situ integration	BGBC; Au; PI[b)]	[77]
TIPS-PEN	11	10^6-10^8		blade-coating	shadow mask	BGTC; Au; Si/SiO_2; PTS[c)]; tested in N_2	[38]
TIPS-PEN	4.6	10^7		blade-coating	shadow mask	BGTC; Au; Si/SiO_2; PTS	[4]
TIPS-PEN	2.7	10^5-10^7		blade-coating	shadow mask	BGTC; Au; Si/SiO_2; PTS; tested in N_2	[73]
TIPS-PEN	1.8	10^7	-10	slot-die coating	shadow mask	BGTC; Au; Si/SiO_2; OTS; tested in air	[90]
TIPS-PEN	1.7	10^5-10^6		inkjet printing	in-situ integration	BGBC; Au/PFBT[d)]; Si/SiO_2	[119]
TIPS-PEN	1.52	10^6	-11	transfer-printing	shadow mask	BGTC; Ag; ITO/SiO_2; tested in air	[36]
TIPS-PEN	1.5	10^5-10^7	~-8	dip-coating	shadow mask	BGTC; Au; Al/Al_2O_3; tested in air	[46]
TIPS-PEN	0.61	10^5	2.1	confined crystallization	shadow mask	BGTC; Au; Si/SiO_2; HMDS[e)]; tested in air	[202]
TIPS-PEN	0.4	~10^4	-6.77	blade-coating	in-situ integration	BGBC; Au; Si/SiO_2; OTS; tested in N_2	[199]
TIPS-PEN	0.36	10^6		template-induced printing	shadow mask	BGTC; Au; Si/SiO_2; tested in air	[138]
TIPS-PEN	0.27	10^6		inkjet printing	in-situ integration	BGBC; Au; Si/SiO_2; HMDS; tested in air	[120]
TIPS-PEN	0.1	10^6	0.69	transfer-printing	shadow mask	BGTC; Au; Si/SiO_2; tested in air	[133]
CuPc	0.02			physical vapor transport	transfer-printing	TGTC; Au; Au/Si_3N_4; tested in air	[29]
CuPc	2.0	10^4	-2	physical vapor transport	transfer-printing	TGTC; Au; Au/Si_3N_4; tested in air	[200]
CuPc	0.04	10^5		transfer-printing	transfer-printing	TGTC; Au; Au/Si_3N_4; tested in air	[130]
C_{10}-BTBT	1.74	10^5	-26	template-guided self-assembly	shadow mask	BGTC; Au; ITO/PI; tested in air	[64]
C_{10}-DNTT[f)]	11	10^6		template-guided self-assembly	shadow mask	BGTC; Au; Si/SiO_2	[71]
Compound 1[g)]	1.26	10^5	-2.6	dip-coating	inkjet printing	BGTC; PEDOT:PSS; Si/SiO_2; PMMA; tested in air	[94]
C_{60}	11	10^5	15-43	template-guided self-assembly	shadow mask	BGTC; Au; Si/SiO_2; BCB[h)]; tested in N_2	[24]
C_{60}	2	10^6	0.5	template-guided self-assembly	shadow mask	BGTC; Au; Si/SiO_2; BCB; tested in N_2	[203]
BPE-PTCDI	0.24	10^5-10^6	~15	filtration-and-transfer	in-situ integration	BGBC; Au; Si/SiO_2; OTS; tested in air	[135]
TCNQ	0.03	10-10^3	0.5	template-guided self-assembly	shadow mask	BGTC; Au; ITO/CL-PVP[i)]	[204]

a) device architectures; S/D electrodes; gate/dielectric; substrate functionalization; test condition; b) PI: polyimide; c) PTS: phenyltrichlorosilane; d) PFBT: pentafluorobenzenethiol; e) HMDS: hexamethyldisilazane; f) C_{10}-DNTT: 2,9-alkyl-dinaphtho[2,3-b:2',3'-f]thieno[3,2-

b]thiophene; g) Compound 1 was synthesized by Pei group in literature[94]; h) BCB: divinyltetramethyldisiloxane bis(benzocyclobutene); i) CL-PVP: cross-linked poly(4-vinylphenol).

In-situ device integration by depositing SMOSN arrays directly onto pre-patterned electrode arrays endows the device with high integration level.[33,77,119,199] Surface modification on electrodes or dielectrics is usually necessary to achieve selective growth of SMOSN within device channels. Large-scale arrays of SMOSN can be directly grown on OTS modified source-drain electrodes during PVD process due to higher surface energy at OTS modified regions, enabling the fabrication of large-scale OFET devices.[33] This method shows good generality and can be applied to a variety of p- and n-type SMOSN.[33] Besides rigid transistors on SiO_2/Si substrates, flexible transistor arrays are also realized by patterned growth of SMOSN on electrode areas on transparent polyethylene terephthalate (PET) substrates.[33] Despite that the performance of rubrene microcrystal-based OFETs presented some degradation on the plastic substrate, no significant loss in performance was observed when the devices were bent to a radius of 6 mm. In another work, by patterning the substrate with solution-wettable and nonwettable regions, selective deposition of C_8-BTBT microcrystals on OFET electrodes was achieved by dropping the solution onto the patterned surface.[77] Self-organized OFETs exhibited an average mobility of 0.53 cm^2 V^{-1} s^{-1} and on/off ratio of 10^9. Inverter circuit fabricated from OFETs also showed a large gain of 20. Recently, a technique termed "controlled organic semiconductor nucleation and extension for circuits" (CONNECT) was also reported for in situ device integration, which combined surface modification and blade-coating method to generate patterned and precisely registered SMOSN within device channels (Figure 17c, d).[199] Transistors density as high as 840 dpi, along with a high yield of 99%, were achieved by this method. The authors further built various logic gates and 2-bit half-adder circuit from the integrated OFETs, verifying the practical applicability of this technique for large-scale circuit applications.

In-situ integration method shows big success and has become a common method to fabricate SMOSN-based OFET arrays via solution method.[33,77,119,199] However, in this method, growth conditions of SMOSN must be very gentle to avoid possible damage of the substrate or pre-patterned electrodes by reaction temperature, therefore limiting its applications on SMOSN that need relatively harsh growth conditions. In addition, nucleation and crystallization of SMOSN can possibly be influenced by the underlying electrodes due to complex organic semiconductor/metal interfaces.[77] Finally, bottom contact OFET configuration may also lead to a large contact resistance, which degrades device performance. To this end, Deng, Zhang and coworkers recently developed a two-step strategy to achieve device integration.[29,130,200] In this strategy, single-crystalline NW arrays were fabricated at a substrate, then electrode arrays which are fabricated by conventional multi-step photolithography were transfer-printed onto these NWs by an etching-assisted transfer printing (ETP) process. In the ETP process, a thin Cu layer was utilized as a sacrificial layer, microelectrodes fabricated on Cu/Si substrate could be readily transferred to diverse conventional or non-conventional substrates with a high transfer yield of near 100%. This transfer printing method exhibits a high flexibility. Various electrodes such as Ti, Au, and Al can be transferred, and various types of organic devices, such as Schottky diodes, resistors, and top-gate OFETs, can be constructed on planar or complex curvilinear substrates. By using this technique, flexible and transparent top-gate OFET arrays with high hole mobility of 2.0 cm^2 V^{-1} s^{-1} were realized (Figure 17e, f).[200] These devices exhibited excellent bending stability with bending radius down to 3 mm. The only concern of this method is that SMOSN have to be exposed to solvent shortly (3 s) during the transfer process. This may lead to possible degradation of SMOSN, therefore fully dry transfer method is desired to improve device performance.

5. Prospective and outlook

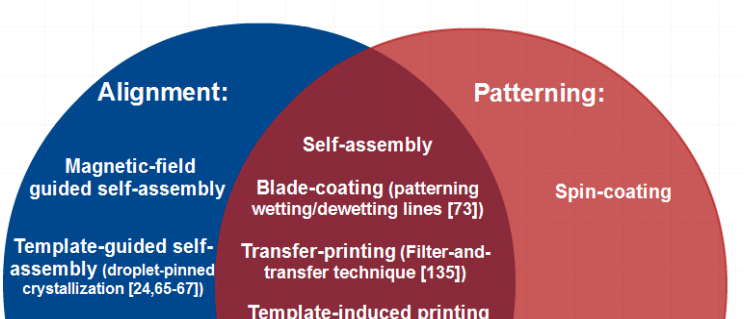

Figure 18. Venn diagram for differnt techniques that developed for alignment and patterning of SMOSN.

SMOSN possess superior electronic and optoelectronic properties and have been identified to be a promising system for device applications like OFETs, photodetectors and optical waveguide. The ability to realize aligned and patterned growth of SMOSN at desired locations with high uniformity is essential for their practical device applications, because disordered systems will cause large variation in device performance and thus very difficult to scale-up for large-area applications.[21,24,37,47] In this review, we focus on the recent advances that have been achieved for controllable assembly of SMOSN into highly ordered arrays and desired patterns at well-defined positions, and discuss their electronic/optoelectronic device applications **(Figure 18)**. A broad range of small molecule organic functional materials have been successfully aligned and patterned on substrate through a wide variety of solution- or vapor-based techniques. Solution-processed methods including coating, printing and self-assembly based methods, hold advantages of low-cost and ease for large-area production,[24] while vapor-processed methods possess the merit of outstanding crystal quality due to clean growth environment.[49] Patterned SMOSN arrays have been successfully applied in high-performance electronic devices including some integrated matrix like image sensors and logic circuits.[50,199]

Despite all these progresses, there are still many problems that need to be addressed before SMOSN can be employed in large-scale industrial applications. First, high-throughput precise positioning of SMOSN at where the electrodes are located or patterned in high accuracy at

desired locations still remains difficult to achieve. Although the reviewed strategies are capable of realizing aligned/patterned growth of SMOSN, there are few reports about the accurate control over their locations and the alignment orientations.[36] Especially the incorporation with high resolution photolithography technique is still hindered by the incompatibility of organic materials with the operation environment of photolithography. Moreover, NW arrays usually can only be aligned in a certain orientation and it is hard to achieve complex patterns which are often required in integrated devices.[4,38,73] The ability of precisely patterning SMOSN determines the yield as well as integration level of SMOSN-based OFETs. Second, patterning/alignment techniques should be applicable to various flexible substrates. Organic materials have the inherent advantage of compatibility with flexible substrates, which makes them a promising system for applications in next-generation wearable and stretchable devices.[10,205-208] However, most of the present patterning techniques involve with organic solvents or high temperature process, and thus cannot be straightforwardly extended to flexible substrates. With the rapid development of flexible electronic devices,[29,45,130] it is highly desirable to realize the growth of aligned/patterned NW arrays on various stretchable and flexible substrates. Third, crystal quality and uniformity of NW arrays need to be improved for high-performance device applications.[36] High quality crystals have less grain boundaries and disorders, and correspondingly can greatly increase charge transport and thus enhance device performance. In addition, uniformity in size, shape and crystallinity of NW arrays can ensure the stability and reproducibility of devices, which are very important aspects for future practical device applications.[9]

Thanks to the rapid development of patterning/alignment techniques, device applications based on SMOSN arrays have made tremendous progress in the last few years. However, several challenges still need to be settled to realize practical applications of SMOSN in organic electronics. First, mobility of SMOSN array-based devices is usually lower than that of single SMOSN-based devices, possibly due to the overlapped organic nanostructures between

electrodes, and the contact issues of semiconductor/electrode or interface issues of insulator/semiconductor. Second, though some device prototypes for integrated devices such as ambipolar transistors, complementary inverters, image sensors and logic circuits have been demonstrated,[50,66,130] the device density and yield need to be significantly improved for electronic circuit applications. Third, device integration should be feasible in a scalable and economical manner, since low cost and large area are key advantages for organic electronics. In spite of these challenges, given the extraordinary properties of SMOSN and the sustained advances in large-scale patterning and device fabrication techniques, it is unambiguous that the applications of SMOSN in organic electronics will have a bright future.

Acknowledgements
This work was supported by the National Basic Research Program of China (Nos. 2013CB933500, 2012CB932400), the Major Research Plan of the National Natural Science Foundation of China (Nos. 91233110, 91333208), and the National Natural Science Foundation of China (Nos. 51172151, 51173124). This work was also sponsored by QinLan project.

Received: ((will be filled in by the editorial staff))
Revised: ((will be filled in by the editorial staff))
Published online: ((will be filled in by the editorial staff))

[1] V. C. Sundar, J. Zaumseil, V. Podzorov, E. Menard, R. L. Willett, T. Someya, M. E. Gershenson, J. A. Rogers, *Science* **2004**, *303*, 1644.

[2] D. J. Gundlach, J. E. Royer, S. K. Park, S. Subramanian, O. D. Jurchescu, B. H. Hamadani, A. J. Moad, R. J. Kline, L. C. Teague, O. Kirillov, C. A. Richter, J. G. Kushmerick, L. J. Richter, S. R. Parkin, T. N. Jackson, J. E. Anthony, *Nat. Mater.* **2008**, *7*, 216.

[3] I. G. Lezama, M. Nakano, N. A. Minder, Z. H. Chen, F. V. D. Girolamo, A. Facchetti, A. F. Morpurgo, *Nat. Mater.* **2012,** *11*, 788.

[4] G. Giri, E. Verploegen, S. C. B. Mannsfeld, S. A. Evrenk, D. H. Kim, S. Y. Lee, H. A. Becerril, A. A. Guzik, M. F. Toney, Z. N. Bao, *Nature* **2011**, *480*, 504.

[5] H. Najafov, B. Lee, Q. Zhou, L. C. Feldman, V. Podzorov, *Nat. Mater.* **2010***, 9,* 938.

[6] T. He, M. Stolte, C. Burschka, N. H. Hansen, T. Musiol, D. Kälblein, J. Pflaum, X. T. Tao, J. Brill, F. Würthner, *Nat. Commun.* **2015***, 6,* 5954.

[7] I. G. Lezama, A. F. Morpurgo, *MRS Bull.* **2013**, *38*, 51.

[8] M. A. Reyes-Martinez, A. J. Crosby, A. L. Briseno, *Nat. Commun.* **2015***, 6,* 6948.

[9] S. Y. Min, T. S. Kim, Y. J. Lee, H. C. Cho, W. T. Xu, T. W. Lee, *Small* **2015**, *11*, 45.

[10] M. Kaltenbrunner, T. Sekitani, J. Reeder, T. Yokota, K. Kuribara, T. Tokuhara, M. Drack, R. Schwödiauer, I. Graz, S. B. Gogonea, S. Bauer, T. Someya, *Nature* **2013**, *499*, 458.

[11] A. N. Sokolov, S. A. Evrenk, R. Mondal, H. B. Akkerman, R. S. S. Carrera, S. G. Focil, J. Schrier, S. C. B. Mannsfeld, A. P. Zoombelt, Z. N Bao, A. A. Guzik, *Nat. Commun.* **2011***, 2*, 437.

[12] C. A. Di, F. J. Zhang, D. B. Zhu, *Adv. Mater*. **2013**, *25*, 313.

[13] J. G. Mei, Y. Diao, A. L. Appleton, L. Fang, Z. N. Bao, *J. Am. Chem. Soc.* **2013**, *135*, 6724.

[14] H. Minemawari, T. Yamada, H. Matsui, J. Tsutsumi, S. Haas, R. Chiba, R. Kumai, T. Hasegawa, *Nature* **2011**, *475*, 364.

[15] P. He, Z. Y. Tu, G. Y. Zhao, Y. G. Zhen, H. Geng, Y. P. Yi, Z. R. Wang, H. T. Zhang, C. H. Xu, J. Liu, X. Q. Lu, X. L. Fu, Q. Zhao, X. T. Zhang, D. Y. Ji, L. Jiang, H. L. Dong, W. P. Hu, *Adv. Mater*. **2015**, *27*, 825.

[16] K. Y. Wu, T. Y. Wu, S. T. Chang, C. S. Hsu, C. L. Wang, *Adv. Mater*. DOI: 10.1002/adma.201501140.

[17] G. Schweicher, V. Lemaur, C. Niebel, C. Ruzié, Y. Diao, O. Goto,W. Y. Lee, Y. Kim, J. B. Arlin, J. Karpinska, A. R. Kennedy, S. R. Parkin, Y. Olivier, S. C. B. Mannsfeld, J. Cornil, Y. H. Geerts, Z. N. Bao, *Adv. Mater*. DOI: 10.1002/adma.201500322.

[18] K. Kim, T. H. Lee, E. J. G. Santos, P. S. Jo, A. Salleo, Y. Nishi, Z. N. Bao, *ACS Nano* DOI: 10.1021/acsnano.5b00581.

[19] C. Zhang, Y. Yan, Y. S. Zhao. J. N. Yao, *Acc. Chem. Res.* **2014**, *47*, 3448.

[20] H. Yu, Z. N. Bao, J. H. Oh, *Adv. Funct. Mater*. **2013**, *23*, 629.

[21] C. Y. Zhang, X. J. Zhang, X. H. Zhang, X. Fan, J. S. Jie, J. C. Chang, C. S. Lee, W. J. Zhang, S. T. Lee, *Adv. Mater*. **2008**, *20*, 1716.

[22] Y. C. Wu, J. G. Feng, X. Y Jiang, Z. Zhang, X. D. Wang, B. Su, L. Jiang, *Nat. Commun.* **2015**, *6*, 6737.

[23] Z. L. Wang, R. R. Bao, X. J. Zhang, X. M. Ou, C. S. Lee, J. C. Chang, X. H. Zhang, *Angew. Chem. Int. Ed*. **2011**, *50*, 2811.

[24] H. Y. Li, B. C. K. Tee, J. J. Cha, Y. Cui, J. W. Chung, S. Y. Lee, Z. N. Bao, *J. Am. Chem. Soc*. **2012**, *134*, 2760.

[25] L. Wei, J. N. Yao, H. B. Fu, *ACS Nano* **2013**, *7*, 7573.

[26] Y. P. Zhang, W. Deng, X. J. Zhang, X. W. Zhang, X. H. Zhang, Y. L. Xing, J. S. Jie, *ACS Appl. Mater. Interfaces* **2013**, *5*, 12288.

[27] R. Saran, V. Stolojan, R. J. Curry, *Sci. Rep.* **2014**, *4*, 5041.

[28] X. J. Zhang, J. S. Jie, W. F. Zhang, C. Y. Zhang, L. B. Luo, Z. B. He, X. H. Zhang, W. J. Zhang, C. S. Lee, S. T. Lee, *Adv. Mater*. **2008**, *20*, 2427.

[29] W. Deng, X. J. Zhang, C. Gong, Q. Zhang, Y. L. Xing, Y. M. Wu, X. W. Zhang, J. S. Jie, *J. Mater. Chem. C* **2014**, *2*, 1314.

[30] R. Ding, J. Feng, X. L. Zhang, W. Zhou, H. H. Fang, Y. F. Liu, Q. D. Chen, H. Y. Wang, H. B. Sun, *Adv. Funct. Mater*. **2014**, *24*, 7085.

[31] V. Podzorov, E. Menard, A. Borissov, V. Kiryukhin, J. A. Rogers, M. E. Gershenson, *Phys. Rev. Lett.* **2004**, *93*, 086602.

[32] C. Reese, Z. N. Bao, *Adv. Mater.* **2007**, *19*, 4535. [33] A, L. Briseno, S. C. B. Mannsfeld, M. M. Ling, S. H. Liu, R. J. Tseng, C. Reese, M. E. Roberts, Y. Yang, F. Wudl, Z. N. Bao, *Nature* **2006**, *444*, 913.

[34] W. S. Zheng, T. Xie, Y. Zhou, Y. L. Chen, W. Jiang, S. L. Zhao, J. X. Wu, Y. M. Jing, Y. Wu, G. C. Chen, Y. F. Guo, J. B. Yin, S. Y. Huang, H. Q. Xu, Z. F. Liu, H. L. Peng, *Nat. Commun.* **2015**, *6*, 6972.

[35] S. Y. Min, T. S. Kim, B. J. Kim, H. Cho, Y. Y. Noh, H. Yang, J. H. Cho, T. W. Lee, *Nat. Commun.* **2013**, *4*, 1773.

[36] K. S. Park, B. Cho, J. Baek, J. K. Hwang, H. Lee, M. M. Sung, *Adv. Funct. Mater*. **2013**, *23*, 4776.

[37] B. Su, Y. C. Wu, L. Jiang, *Chem. Soc. Rev*. **2012**, *41*, 7832.

[38] Y. Diao, B. C. K. Tee, G. Giri, J. Xu, D. H. Kim, H. A. Becerril, R. M. Stoltenberg, T. H. Lee, G. Xue, S. C. B. Mannsfeld, Z. N. Bao, *Nat. Mater.* **2013**, *12*, 665.

[39] X. Y. Zheng, H. Geng, Y. P. Yi, Q. K. Li, Y. Q. Jiang, D. Wang, Z. G. Shuai, *Adv. Funct. Mater*. **2014**, *24*, 5531.

[40] D. W. He, Y. H. Zhang, Q. S. Wu, R. Xu, H. Y. Nan, J. F. Liu, J. Y. Yao, Z. L. Wang, S. J. Yuan, Y. Li, Y. Shi, J. L. Wang, Z. H. Ni, L. He, F. Miao, F. Q. Song, H. X. Xu, K. Watanabe, T. Taniguchi, J. B. Xu, X. R. Wang, *Nat. Commun.* **2014**, *5*, 5162.

[41] P. Campbell, *The Science and Engineering of Micro-electronic Fabrication*, Oxford University Press, New York, USA **1996**, pp. 11-31.

[42] Q. Michael, *Semiconductor manufacturing Technology*, Pearson Education Press, London, UK **2001**, pp. 341-378

[43] R. Dammel, *Diazonaphthoquinone-Based Resists*, Optical Engineering Press, Bellingham, USA **1993**, pp. 10-40.

[44] K. Nakayama, M. Uno, T. Uemura, N. Namba, Y. Kanaoka, T. Kato, M. Katayama, C. Mitsui, T. Okamoto, J. Takeya, *Adv. Mater. Interfaces* **2014**, *1*, 1300124.

[45] D. Y. Ji, L. F. Jiang, L. Jiang, X. L. Fu, H. L. Dong, J. S. Yu, W. P. Hu, *Chem. Commun.* **2014**, *50*, 8328.

[46] J. Jang, S. Nam, K. Im, J. Hur, S. N. Cha, J. Kim, H. B. Son, H. Suh, M. A. Loth, J. E. Anthony, J. J. Park, C. E. Park, J. M. Kim, K. Kim, *Adv. Funct. Mater.* **2012**, *22*, 1005.

[47] L. Jiang, H. L. Dong, W. P. Hu, *Soft Matter* **2011**, *7*, 1615.

[48] Q. H. Cui, L. Jiang, C. Zhang, Y. S. Zhao, W. P. Hu, J. N. Yao, *Adv. Mater*. **2012**, *24*, 2332.

[49] M. Wang, J. Li, G. Y. Zhao, Q. H. Wu, Y. G. Huang, W. P. Hu, X. K. Gao, H. X. Li, D. B. Zhu, *Adv. Mater*. **2013**, *25*, 2229.

[50] Y. M. Wu, X. J. Zhang, H. H. Pan, W. Deng, X. H. Zhang, X. W. Zhang, J. S. Jie, *Sci. Rep.* **2013**, *3*, 3248.

[51] C. L. Wang, H. L. Dong, W. P. Hu, Y. Q. Liu, D. B. Zhu, *Chem. Rev.* **2012**, *112*, 2208.

[52] K. Tseng, Y. Tsai, C. Wu, J. Shyue, D. M. Bassani, K. Wong, *Chem. Commun.* **2013**, *49*, 11536.

[53] E. D. Głowacki, M. Irimia-Vladu, M. Kaltenbrunner, J. Gsiorowski, M. S. White, U. Monkowius, G. Romanazzi, G. P. Suranna, P. Mastrorilli, T. Sekitani, S. Bauer, T. Someya, L. Torsi, N. S. Sariciftci, *Adv. Mater.* **2013**, *25*, 1563.

[54] E. D. Glowacki, L. Leonat, M. Irimia-Vladu, R. S. Diauer, M. Ullah, H. Sitter, S. Bauer, N. S. Sariciftci, *Appl. Phys. Lett.* **2012**, *101*, 023305.

[55] X. J. Zhang, X. H. Zhang, B. Wang, C. Y. Zhang, J. C. Chang, C. S. Lee, S. T. Lee, *J. Phys. Chem. C* **2008**, *112*, 16264.

[56] X. J. Zhang, X. H. Zhang, W. S. Shi, X. M. Meng, C. S. Lee, S. T. Lee, *Angew. Chem. Int. Ed.* **2007**, *46*, 1525.

[57] Q. X. Tang, H. X. Li, M. He, W. P. Hu, C. M. Liu, K. Q. Chen, C. Wang, Y. Q. Liu, D. B. Zhu, *Adv. Mater.* **2006**, *18*, 65.

[58] S. H. Liu, W. M. Wang, A. L. Briseno, S. C. B. Mannsfeld, Z. N. Bao, *Adv. Mater.* **2009**, *21*, 1217.

[59] C. Y. Zhang, X. J. Zhang, X. H. Zhang, X. M. Ou, W. F. Zhang, J. S. Jie, J. C. Chang, C. S. Lee, S. T. Lee, *Adv. Mater.* **2009**, *21*, 4172.

[60] Y. L. Xing, W. Deng, H. Wang, C. Gong, X. J. Zhang, J. S. Jie, *J. Nanosci. Nanotechnol.* **2014**, *15*, 4450.

[61] M. Cavallini, P. D'Angelo, V. V. Criado, D. Gentili, A. Shehu, F. Leonardi, S. Milita, F. Liscio, F. Biscarini, *Adv. Mater.* **2011**, *23*, 5091.

[62] X. X. Duan, Y. P. Zhao, E. Berenschot, N. R. Tas, D. N. Reinhoudt, J. Huskens, *Adv. Funct. Mater.* **2010**, *20*, 2519.

[63] P. S. Jo, A. Vailionis, Y. M. Park, A. Salleo, *Adv. Mater.* **2012**, *24*, 3269.

[64] A. Kim, K. Jang, J. Kim, J. C. Won, M. H. Yi, H. Kim, D. K. Yoon, T. J. Shin, M. Lee, J. Ka, Y. H. Kim, *Adv. Mater.* **2013**, *25*, 6219.

[65] H. Y. Li, B. C.-K. Tee, G. Giri, J. W. Chung, S. Y. Lee, Z. N. Bao, *Adv. Mater.* **2012**, *24*, 2588.

[66] C. C. Fan, A. P. Zoombelt, H. Jiang, W. F. Fu, J. K. Wu, W. T. Yuan, Y. Wang, H. Y. Li, H. Z. Chen, Z. N. Bao, *Adv. Mater.* **2013**, *25*, 5762.

[67] J. K. Wu, C. C. Fan, G. B. Xue, T. Ye, S. Liu, R. Q. Lin, H. Z. Chen, H. L. Xin, R. Xiong, H. Y. Li, *Adv. Mater.* DOI: 10.1002/adma.201501577.

[68] B. Mukherjee, K. Sim, T. J. Shin, J. Lee, M. Mukherjee, M. Reec, S. Pyo, *J. Mater. Chem.* **2012**, *22*, 3192.

[69] R. R. Bao, C. Y. Zhang, Z. L. Wang, X. J. Zhang, X. M. Ou, C. S. Lee, J. S. Jie, X. H. Zhang, *Chem. Eur. J.* **2012**, *18*, 975.

[70] D. H. Kim, J. A. Lim, W. Cha, J. H. Lee, H. Kim, J. H. Cho, *Org. Electron.* **2014**, *15*, 2322.

[71] K. Nakayama, Y. Hirose, J. Soeda, M. Yoshizumi, T. Uemura, M. Uno, W. Y. Li, M. J. Kang, M. Yamagishi, Y. Okada, E. Miyazaki, Y. Nakazawa, A. Nakao, K. Takimiya, J. Takeya, *Adv. Mater.* **2011**, *23*, 1626.

[72] R. R. Bao, C. Y. Zhang, X. J. Zhang, X. M. Ou, C. S. Lee, J. S. Jie, X. H. Zhang, *ACS Appl. Mater. Interfaces* **2013**, *5*, 5757.

[73] G. Giri, S. Park, M. Vosgueritchian, M. M. Shulaker, Z. N. Bao, *Adv. Mater.* **2014**, *26*, 487.

[74] Y. Li, C. Liu, A. Kumatani, P. Darmawan, T. Minari, K. Tsukagoshi, *Org. Electron.* **2012**, *13*, 264.

[75] O. Goto, S. Tomiya, Y. Murakami, A. Shinozaki, A. Toda, J. Kasahara, D. Hobara, *Adv. Mater.* **2012**, *24*, 1117.

[76] Y. Li, C. Liu, A. Kumatani, P. Darmawan, T. Minari, K. Tsukagoshi, *AIP Advances* **2011**, *1*, 022149.

[77] T. Minari, M. Kano, T. Miyadera, S. D. Wang, Y. Aoyagi, K. Tsukagoshi, *Appl. Phys. Lett.* **2009**, *94*, 093307.

[78] K. Kotsuki, S. Obata, K. Saiki, *Langmuir* **2014**, *30*, 14286.

[79] M. Yoshio, Y. Shoji, Y. Tochigi, Y. Nishikawa, T. Kato, *J. Am. Chem. Soc.* **2009**, *131*, 6763.

[80] Y. Shoji, M. Yoshio, T. Yasuda, M. Funahashi, T. Kato, *J. Mater. Chem.* **2010**, *20*, 173.

[81] C. Gong, W. Deng, B. Zou, Y. L. Xing, X. J. Zhang, X. H. Zhang, J. S. Jie, *ACS Appl. Mater. Interfaces* **2014**, *6*, 11018.

[82] K. Takazawa, J. Inoue, K. Mitsuishi, *Nanoscale* **2014**, *6*, 4174.

[83] I. O. Shklyarevskiy, P. Jonkheijm, P. C. M. Christianen, A. P. H. J. Schenning, A. D. Guerzo, J. Desvergne, E. W. Meijer, J. C. Maan, *Langmuir* **2005**, *21*, 2108.

[84] F. J. Zhang, C. A. Di, N. Berdunov, Y. Y. Hu, Y. B. Hu, X. K. Gao, Q. Meng, H. Sirringhaus, D. B. Zhu, *Adv. Mater.* **2013**, *25*, 1401.

[85] Y. Yuan, G. Giri, A. L. Ayzner, A. P. Zoombelt, S. C. B. Mannsfeld, J. Chen, D. Nordlund, M. F. Toney, J. Huang, Z. Bao. *Nat. Commun*. **2014**, *5*,3305

[86] F. Liu, S. Ferdous, E. Schaible, A. Hexemer, M. Church, X. D. Ding, C. Wang, T. P. Russell, *Adv. Mater.* **2015**, 27, 886.

[87] Q. Meng, F. J. Zhang, Y. P. Zang, D. Z. Huang, Y. Zou, J. Liu, G. Y. Zhao, Z. R. Wang, D. Y. Ji, C. A. Di, W. P. Hu, D. B. Zhu, *J. Mater. Chem. C* **2014**, *2*, 1264.

[88] J. Lee, A. R Han, J. Hong, J. H. Seo, J. H. Oh, C. Yang, *Adv. Funct. Mater*. **2012**, *22*, 4128.

[89] A. Pierre, M. Sadeghi, M. M. Payn, A. Facchett, J. E. Anthony, A. C. Arias, *Adv. Mater.* **2014**, *26*, 5722.

[90] J. J. Chan, C. Y. Chi, J. Zhang, J. S. Wu, *Adv. Mater*. **2013**, *25*, 6442.

[91] W. Ma, J. Reinspach, Y. Zhou, Y. Diao, T. McAfee, S. C. B. Mannsfeld, Z. N. Bao, H. Ade, *Adv. Funct. Mater*. DOI: 10.1002/adfm.201500468.

[92] S. Nam, J. Jang, J. E. Anthony, J.-J. Park, C. E. Park, K. Kim, *ACS Appl. Mater. Interfaces* **2013**, *5*, 2146.

[93] L. Q. Li, P. Gao, W. C. Wang, K. Müllen, H. Fuchs, L. F. Chi, *Angew. Chem. Int. Ed*. **2013**, *52*, 12530.

[94] N. L. Liu, Y. Zhou, N. Ai, C. Luo, J. B. Peng, J. Wang, J. Pei, Y. Cao, *Langmuir* **2011**, *27*, 14710.

[95] G. P. Chang, K. H. Hsieh, *Synth. Met*. **2013**, *165*, 1.

[96] T. P. Corrales, M. Bai, V. D. Campo, P. Homm, P. Ferrari, A. Diama, C. Wagner, H. Taub, K. Knorr, M. Deutsch, M. J. Retamal, U. G. Volkmann, P. Huber, *ACS Nano* **2014**, *8*, 9954.

[97] L. Shan, D. Q. Liu, H. Li, X. M. Xu, B. W. Shan, J. B. Xu, Q. Miao, *Adv. Mater*. DOI: 10.100/adma.201500149.

[98] N. L. Liu, Y. Zhou, L. Wang, J. B. Peng, J. Wang, J. Pei, Y. Cao, *Langmuir* **2009**, 25, 665.

[99] Y. H. Tong, Q. X. Tang, H. T. Lemke, K. Moth-Poulsen, F. Westerlund, P Hammershøj, K. Bechgaard, W. P. Hu, T. Bjørnholm, *Langmuir* **2010**, *26*, 1130.

[100] R. Z. Rogowski, A. Dzwilewski, M. Kemerink, A. A. Darhuber, *J. Phys. Chem. C* **2011**, *115*, 11758.

[101] L. Q. Li, P. Gao, K. C. Schuermann, S. Ostendorp, W. C. Wang, C. Du, Y. Lei, H. Fuchs, L. D. Cola, K. Müllen, L. F. Chi, *J. Am. Chem. Soc.* **2010**, *132*, 8807.

[102] L. Q. Li, P. Gao, M. Baumgarten, K. Müllen, N. Lu, H. Fuchs, L. F. Chi, *Adv. Mater.* **2013**, *25*, 3419.

[103] M. M. Li, C. B. An, W. Pisula, K. Müllen, *Small* **2014**, *10*, 1926.

[104] T. Sakanoue, H. Sirringhaus, *Nat. Mater.* **2010**, *9*, 736.

[105] Y. Li, C. Liu, Y. Xu, T. Minari, P. Darmawan, K. Tsukagoshi, *Org. Electron.* **2012**, *13*, 815.

[106] Y. Li, C. Liu, M. V. Lee, Y. Xu, X. Wang, Y. Shi, K. Tsukagoshi, *J. Mater. Chem. C* **2013**, *1*, 1352.

[107] J. J. van Franeker, D. Westhoff, M. Turbiez, M. M. Wienk, V. Schmidt, R. A. J. Janssen, *Adv. Funct. Mater.* **2015**, *25*, 855.

[108] H. L. Chen, S. H. Dong, M. L. Bai, N. Y. Cheng, H. Wang, M. L. Li, H. W. Du, S. X. Hu, Y. L. Yang, T. Y. Yang, F. Zhang, L. Gu, S. Meng, S. M. Hou, X. F. Guo. *Adv. Mater.* **2015**, *27*, 2113.

[109] Y. Li, C. Liu, Y. Wang, Y. Yang, X. R. Wang, Y. Shi, K. Tsukagoshi, *AIP Advances* **2013**, *3*, 052123.

[110] D. Choi, B. Ahn, S. H. Kim, K. Hong, M. Ree, C. E. Park, *ACS Appl. Mater. Interfaces* **2012**, *4*, 117.

[111] Z. H. Liu, H. A. Becerril, M. E. Roberts, Y. Nishi, Z. N. Bao, *IEEE Trans. Elec. Dev.* **2009**, *56*, 176.

[112] J. Soeda, T. Uemura, T. Okamoto, C. Mitsui, M. Yamagishi, J. Takeya, *Appl. Phys. Express*. **2013**, *6*, 076503.

[113] G. Giri, E. Miller, Z. Bao, *J. Mater. Res.* **2014,** *29*, 2615.

[114] H. A. Becerril, M. E. Roberts, Z. H. Liu, J. Locklin, Z. N. Bao, *Adv. Mater*. **2008**, *20*, 2588.

[115] Z. Y. Fan, J. C. Ho, T. Takahashi, R. Yerushalmi, K. Takei, A. C. Ford, Y. L. Chueh, A. Javey, *Adv. Mater*. **2009**, *21*, 3730.

[116] H. Yan, Z. H. Chen, Y. Zheng, C. Newman, J. R. Quinn, F. Dotz, M. Kastler, A. Facchetti, *Nature* **2009**, *457*, 679.

[117] M. Singh, H. M. Haverinen, P. Dhagat, G. E. Jabbour, *Adv. Mater.* **2010**, *22*, 673.

[118] M. Kuang, L. B. Wang, Y. L. Song, *Adv. Mater.* **2014**, *26*, 6950.

[119] Y. H. Kim, B. Yoo, J. E. Anthony, S. K. Park, *Adv. Mater.* **2012**, *24*, 497.

[120] J. A. Lim, W. H. Lee, H. S. Lee, J. H. Lee, Y. D. Park, K. Cho, *Adv. Funct. Mater.* **2008**, *18*, 229.

[121] A. Carlson, A. M. Bowen, Y. G. Huang, R. G. Nuzzo, J. A. Rogers, *Adv. Mater.* **2012**, *24*, 5284.

[122] T. Takahashi, K. Takei, J. C. Ho, Y. L. Chueh, Z. Y. Fan, A. Javey, *J. Am. Chem. Soc.* **2009**, *131*, 2102.

[123] C. H. Lee, D. R. Kim, X. L. Zheng, *Proc. Natl. Acad. Sci. USA* **2010**, *107*, 9950.

[124] C. H. Lee, D. R. Kim, X. L. Zheng, *Nano Lett.* **2011**, *11*, 3435.

[125] Q. N. Thanh, H. Jeong, J. Kim, J. W. Kevek, Y. H. Ahn, S. Lee, E. D. Minot, J. Y. Park, *Adv. Mater.* **2012**, *24*, 4499.

[126] Z. Y. Fan, J. C. Ho, Z. A. Jacobson, R. Yerushalmi, R. L. Alley, H. Razavi, A. Javey, *Nano Lett.* **2008**, *8*, 20.

[127] R. Yerushalmi, Z. A. Jacobson, J. C. Ho, Z. Y. Fan, A. Javey, *Appl. Phys. Lett.* **2007**, *91*, 203104.

[128] J. K. Hwang, S. Cho, J. M. Dang, E. B. Kwak, K. Song, J. Moon, M. M. Sung, *Nat. Nanotechnol.* **2010**, *5*, 742.

[129] K. S. Park, S. M. Salunkhe, I. Lim, C. Cho, S. H. Han, M. M. Sung, *Adv. Mater.* **2013**, *25*, 3351.

[130] W. Deng, X. J. Zhang, H. H. Pan, Q. X. Shang, J. C. Wang, X. H. Zhang, X. W. Zhang, J. S. Jie, *Sci. Rep.* **2014**, *4*, 5358.

[131] G. W. Hsieh, J. J. Wang, K. Ogata, J. Robertson, S. Hofmann, W. I. Milne, *J. Phys. Chem. C* **2012**, *116*, 7118.

[132] K. S. Park, K. S. Lee, C. Kang, J. Baek, K. S. Han, C. Lee, Y. K. Lee, Y. Kang, M. M. Sung, *Nano Lett.* **2015**, *15*, 289.

[133] K. Lee, J. Kim, K. Shin, Y. S. Kim, *J. Mater. Chem.* **2012**, *22*, 22763.

[134] Y. P. Zhang, X. D. Wang, Y. M. Wu, J. S. Jie, X. W. Zhang, Y. L. Xing, H. H. Wu, B. Zou, X. J. Zhang, X. H. Zhang, *J. Mater. Chem.* **2012**, *22*, 14357.

[135] J. H. Oh, H. W. Lee, S. Mannsfeld, R. M. Stoltenberg, E. Jung, Y. W. Jin, J. M. Kim, J.-B. Yoo, Z. N. Bao, *Proc. Natl. Acad. Sci. USA* **2009**, *106*, 6065.

[136] B. D. Gates, Q. B. Xu, M. Stewart, D. Ryan, C. G. Willson, G. M. Whitesides, *Chem. Rev.* **2005**, *105*, 1171.

[137] M. Cavallini, C. Albonetti, F. Biscarini, *Adv. Mater.* **2009**, *21*, 1043.

[138] I. Bae, S. J. Kang, Y. J. Shin, Y. J. Park, R. H. Kim, F. Mathevet, C. Park, *Adv. Mater.* **2011**, *23*, 3398.

[139] I. Bae, S. K. Hwang, R. H. Kim, S. J. Kang, C. Park, *ACS Appl. Mater. Interfaces* **2013**, *5*, 10696.

[140] H. B. Liu, Y. L. Li, S. Q. Xiao, H. Y. Gan, T. G. Jiu, H. M. Li, L. Jiang, D. B. Zhu, D. P. Yu, B. Xiang, Y. F. Chen, *J. Am. Chem. Soc.* **2003**, *125*, 10794.

[141] Q. H. Cui, Y. S. Zhao, J. N. Yao, *Adv. Mater.* **2014**, *26*, 6852.

[142] H. Jiang, H. P. Zhao, K. K. Zhang, X. D. Chen, C. Kloc, W. P. Hu, *Adv. Mater.* **2011**, *23*, 5075.

[143] H. Wang, Y. Zhao, Z. Q. Xie, H. Shang, H. Y. Wang, F. Li, Y. G. Ma, *CrystEngComm* **2015**, *17*, 2168.

[144] Y. X. Xu, H. Y. Zhang, F. Li, F. Z. Shen, H. Wang, X. J. Li, Y. Yu, Y. G. Ma, *J. Mater. Chem.* **2012**, *22*, 1592.

[145] Y. W. Huang, R. J. Yuan, S. M. Zhou, *J. Mater. Chem.* **2012**, *22*, 883.

[146] Y. S. Zhao, J. S. Wu, J. X. Huang, *J. Am. Chem. Soc.* **2009**, *131*, 3158.

[147] Y. S. Zhao, P. Zhan, J. Kim, C. Sun, J. X. Huang, *ACS Nano* **2010**, *4*, 1630.

[148] J. W. Chung, B. An, J. W. Kim, J. Kim, S. Y. Park, *Chem. Commun.* **2008**, 2998.

[149] B. N. Mbenkum, E. Barrena, X. N. Zhang, M. Kelsch, H. Dosch, *Nano Lett.* **2006**, *6*, 2852.

[150] T. N. Krauss, E. Barrena, T. Lohmüller, M. Kelsch, A. Breitling, P. A. V. Aken, J. P. Spatz, H. Dosch, *Chem. Mater.* **2009**, *21*, 5010.

[151] N. Y. J. Phillipp, T. N. Krauss, P. A. V. Aken, *ACS Nano* **2012**, *6*, 4039.

[152] Y. M. Wu, X. J. Zhang, H. H. Pan, X. W. Zhang, Y. P. Zhang, X. Z. Zhang, J. S. Jie, *Nanotechnology* **2013**, *24*, 355201.

[153] H. H. Pan, X. J. Zhang, Y. Yang, Z. B. Shao, W. Deng, K. Ding, Y. Zhang, J. S. Jie, *Nanotechnology* **2015,** *26*, 295302.

[154] M. Engel, M. Steiner, P. Avouris, *Nano Lett*. **2014**, *14*, 6414.

[155] A. Pospischil, M. Humer, M. M. Furchi, D. Bachmann, R. Guider, T. Fromherz, T. Mueller, *Nat. Photonics.* **2013**, *7*, 892.

[156] M. Furchi, A. Urich, A. Pospischil, G. Lilley, K. Unterrainer, H. Detz, P. Klang, A. M. Andrews, W. Schrenk, G. Strasser, T. Mueller, *Nano Lett.* **2012**, *12*, 2773.

[157] F. Guo, B. Yang, Y. B. Yuan, Z. G. Xiao, Q. F. Dong, Y. Bi, J. S. Huang, *Nat. Nanotechnol.* **2012**, *7*, 798.

[158] W. D. Li, S. Y. Chou, *Opt. Express* **2010**, *18*, 931.

[159] H. L. Dong, H. F. Zhu, Q. Meng, X. Gong, W. P. Hu, *Chem. Soc. Rev.* **2012**, *41*, 1754.

[160] K. J. Baeg, M. Binda, D. Natali, M. Caironi, Y. Y. Noh, *Adv. Mater.* **2013**, *25*, 4267.

[161] T. Y. Zhai, L. Li, X. Wang, X. S. Fang, Y. Bando, D. Golberg, *Adv. Funct. Mater.* **2010**, *20*, 4233.

[162] T. Y. Zhai, L. Li, Y. Ma, M. Y. Liao, X. Wang, X. S. Fang, J. N. Yao, Y. Bando, D. Golberg, *Chem. Soc. Rev.* **2011**, *40*, 2986.

[163] L. Wang, J. S. Jie, Z. B. Shao, Q. Zhang, X. H. Zhang, Y. M. Wang, Z. Sun, S. T. Lee, *Adv. Funct. Mater.* **2015**, *25*, 2910.

[164] H. Najafov, B. Lee, Q. Zhou, L. C. Feldman, V. Podzorov, *Nat. Mater.* **2010**, *9*, 938.

[165] A. T. Haedler, K. Kreger, A. Issac, B. Wittmann, M. Kivala, N. Hammer, J. Kohler, H. W. Schmidt, R. Hildner, *Nature* **2015**, *523*, 196.

[166] J. C. Bolinger, M. C. Traub, T. Adachi, P. F. Barbara, *Science* **2011**, *331*, 565.

[167] J. Vogelsang, T. Adachi, J. Brazard, D. A. V. Bout, P. F. Barbara, *Nat. Mater.* **2011**, *10*, 942.

[168] X. Gong, M. H. Tong, Y. J. Xia, W. Z. Cai, J. S. Moon, Y. Cao, G. Yu, C. L. Shieh, B. Nilsson, A. J. Heeger, *Science* **2009**, *325*, 1665.

[169] L. T. Dou, Y. Yang, J. B. You, Z. R. Hong, W. H. Chang, G. Li, Y. Yang, *Nat. Commun*. **2014**, *5*, 5404.

[170] N. Ai, Y. Zhou, Y. N. Zheng, H. B. Chen, J. Wang, J. Pei, Y. Cao, *Org. Electron.* **2013**, *14*, 1103.

[171] W. Deng, J. S. Jie, Q. X. Shang, J. C. Wang, X. J. Zhang, S. W. Yao, Q. Zhang, X. H. Zhang, *ACS Appl. Mater. Interfaces* **2015**, *7*, 2039.

[172] Q. X. Tang, L. Q. Li, Y. B. Song, Y. L. Liu, H. X. Li, W. Xu, Y. Q. Liu, W. P. Hu, D. B. Zhu, *Adv. Mater.* **2007**, *19*, 2624.

[173] Y. S. Kim, S. Y. Bae, K. H. Kim, T. W. Lee, J. A. Hur, M. H. Hoang, M. J. Cho, S. J. Kim, Y. Kim, M. Kim, K. Lee, S. J. Lee, D. H. Choi, *Chem. Commun.* **2011**, *47*, 8907.

[174] J. Kim, S. Cho, Y. H. Kim, S. K. Park, *Org. Electron.* **2014**, *15*, 2099.

[175] K. H. Kim, S. Y. Bae, Y. S. Kim, J. A. Hur, M. H. Hoang, T. W. Lee, M. J. Cho, Y. Kim, M. Kim, J. Jin, S. J. Kim, K. Lee, S. J. Lee, D. H. Choi, *Adv. Mater.* **2011**, *23*, 3095.

[176] B. Mukherjee, M. Mukherjee, K. Sim, S. Pyo, *J. Mater. Chem.* **2011**, *21*, 1931.

[177] S. Nau, C. Wolf, S. Sax, E. J. W. L. Kratochvil, *Adv. Mater.* **2015**, *27*, 1048.

[178] E. Ozgur, O. Aktas, M. Kanik, M. Yaman, M. Bayindir, *Nano Lett.* **2012**, *12*, 2483.

[179] Z. Y. Fan, J. C. Ho, Z. A. Jacobson, H. Razavi, A. Javey, *Proc. Natl. Acad. Sci. USA* **2008**, *105*, 11066.

[180] G. H. Gelinck, H. E. A. Huitema, E. van Veenendaal, E. Cantatore, L. Schrijnemakers, J. B. P. H. van der Putten, T. C. T. Geuns, M. Beenhakkers, J. B. Giesber, B. H. Huisman, E. J. Meijer, E. M. Benito, F. J. Touwslager, A. W. Marsman, B. J. E. van Rens, D. M. de Leeuw, *Nat. Mater*. **2004**, *3*, 106.

[181] J. L. Zhang, C. Wang, C. W. Zhou, *ACS Nano* **2012**, *6*, 7412.

[182] B. Comiskey, J. D. Albert, H. Yoshizawa, J. Jacobson, *Nature* **1998**, *394*, 253.

[183] J. A. Rogers, Z. N. Bao, K. Baldwin, A. Dodabalapur, B. Crone, V. R. Raju, V. Kuck, H. Katz, K. Amundson, J. Ewing, P. Drzaic, *Proc. Natl Acad Sci USA* **2011**, *98*, 4835.

[184] G. Y. Zhao, H. L. Dong, L. Jiang, H. P. Zhao, X. Qin, W. P. Hu, *Appl. Phys. Lett*. **2012**, *10*, 103302.

[185] Y. B. Zeng, W. Huang , W. Shi, J. S. Yu, *Appl. Phys.*A **2015**, *118*, 1279.

[186] V. Subramanian, J. M. J. Fréchet, P. C. Chang, D. C. Huang, J. B. Lee, S. E. Molesa, A. R. Murphy, D. R. Redinger, S. K. Volkman, *Proc. IEEE* **2005**, *93*, 1330.

[187] R. Rotzoll, S. Mohapatra, V. Olariu, R. Wenz, M. Grigas, K. Dimmler, O. Shchekin, A. Dodabalapur, *Appl. Phys. Lett*. **2006**, *88*, 123502.

[188] E. Meenard, V. Podzorov, S.-H. Hur, A. Gaur, M. E. Gershenson, J. A. Rogers, *Adv. Mater*. **2004**, *16*, 23.

[189] J. Takeya, M. Yamagishi, Y. Tominari, R. Hirahara, Y. Nakazawa, T. Nishikawa, T. Kawase, T. Shimoda, S. Ogawa, *Appl. Phys. Lett*. **2007**, *90*, 102120.

[190] O. D. Jurchescu, M. Popinciuc, B. J. van Wees, T. T. M. Palstra, *Adv. Mater*. **2007**, *19*, 688.

[191] G. Schweicher, V. Lemaur, C. Niebel, C. Ruzié, Y. Diao, O. Goto, W. Y. Lee, Y. Kim, J. B. Arlin, J. Karpinska, A. R. Kennedy, S. R. Parkin, Y. Olivie, S. C. B. Mannsfeld, J. Cornil, Y. H. Geerts, Z. N. Bao, *Adv. Mater*. **2015**, *27*, 3066.

[192] C. Liu, T. Minari, X. B. Lu, A. Kumatani, K. Takimiya, K. Tsukagoshi, *Adv. Mater*. **2011**, *23*, 523.

[193] Y. S. Yang, T. Yasuda, H. Kakizoe, H. Mieno, H. Kino, Y. Tateyama, C. Adachi, *Chem. Commun*. **2013**, *49*, 6483.

[194] M. Ichikawa, T. Kato, T. Uchino, T. Tsuzuki, M. Inoue, H. G. Jeon, T. Koyama, Y. Taniguchi, *Org. Electron*. **2010**, *11*, 1549.

[195] C. L. Wang, Z. X. Liang, Y. L. Liu, X. M. Wang, N. Zhao, Q. Miao, W. P. Hu, J. B. Xu, *J. Mater. Chem*. **2011**, *21*, 15201.

[196] C. M. Liu, C. Y. Xiao, Y. Li, W. P. Hu, Z. B. Li, Z. H. Wang, *Chem. Commun*. **2014**, *50*, 12462.

[197] L. Q. Li, Q. X. Tang, H. X. Li, X. D. Yang, W. P. Hu, Y. B. Song, Z. G. Shuai, W. Xu, Y. Q. Liu, D. B. Zhu, *Adv. Mater*. **2007**, *19*, 2613.

[198] T. He, M. Stolte, F. Würthner, *Adv. Mater*. **2013**, *25*, 6951.

[199] S. Park, G. Giri, L. Shaw, G. Pitner, J. Ha, J. H. Koo, X. D. Gu, J. Park, T. H. Lee, J. H. Nam, Y. Hong, Z. N. Bao, *Proc. Natl Acad Sci USA* **2015**, *112*, 5561.

[200] W. Deng, X. J. Zhang, J. C. Wang, Q. X. Shang, C. Gong, X. H. Zhang, Q. Zhang, J. S. Jie, *Org. Electron.* **2014**, *15*, 1317.

[201] J.-H. Kim, S. H. Hong, K.-d. Seong, S. Seo, *Adv. Funct. Mater.* **2014**, *24*, 2404.

[202] H. B. Akkerman, A. C. Chang, E. Verploegen, C. J. Bettinger, M. F. Toney, Z. N. Bao, *Org. Electron.* **2012,** *13*, 235.

[203] H. Y. Li, C. C. Fan, M. Vosgueritchian, B. C.-K. Tee, H. Z. Chen, *J. Mater. Chem. C* **2014**, *2*, 3617.

[204] B. Mukherjee, T. J. Shin, K. Sim, M. Mukherjee, J. Lee, S. H. Kim, S. Pyo, *J. Mater. Chem*. **2010**, *20*, 9047.

[205] A. Campana, T. Cramer, D. T. Simon, M. Berggren, F. Biscarini, *Adv. Mater*. **2014**, *26*, 3874.

[206] C. M. Lochner, Y. Khan, A. Pierre, A. C. Arias, *Nat. Commun.* **2014***, 5,* 5745.

[207] A. K. Bansal, S. B. Hou, O. Kulyk, E. M. Bowman, I. D. W. Samuel, *Adv. Mater.* DOI: 10.1002/adma.201403560.

[208] G. Schwartz, B. C. K. Tee, J. G. Mei, A. L. Appleton, D. H. Kim, H. L. Wang, Z. N. Bao, *Nat. Commun.* **2013***, 4*, 1859.

Xiujuan Zhang received her Ph. D. degree in chemistry from Technical Institute of Physics and Chemistry, Chinese Academy of Sciences (CAS) in 2006. After that, she worked as a postdoctoral fellow at City University of Hong Kong. In 2009, she joined institute of Functional Nano & Soft Materials (FUNSOM), Soochow University. Her research involves design and synthesis of small-molecule organic micro/nanocrystals and their applications in opto/electronic devices.

Jiansheng Jie received his B. S. and Ph. D. degree in physics from University of Science and Technology of China (USTC) in 1999 and 2004 respectively. He then went to Prof. Shuit-tong Lee‘s lab as a postdoctoral fellow at City University of Hong Kong. After that, he started to work at Hefei University of Technology as a professor in 2006. In 2010, he joined Institute of Functional Nano & Soft Materials (FUNSOM), Soochow University. His research focuses on synthesis of organic and inorganic nanostructures for their applications in flexible electronics, optoelectronics, and solar energy conversion devices.

Xiaohong Zhang received his B. S. and M. S. degree at Beijing University of Aeronautics and Astronautics in 1989 and 1992, respectively. He obtained his Ph. D. degree at Beijing Institute of Technology in 1996. After that, he worked as post-doctor at Institute of Photographic Chemistry of Chinese Academy of Sciences (CAS), and City University of Hong Kong respectively. He joined Technical Institute of Physics and Chemistry of CAS as a professor in 2000. Since 2013, he came to Institute of Functional Nano & Soft Materials (FUNSOM), Soochow University, as a professor. His research interests include organic optoelectronic materials, semiconductor nanomaterials and optoelectronic devices.

Large-area aligning and patterning of small-molecule organic semiconductor micro/nanocrystals (SMOSN) at desired locations is prerequisite for their device applications in practice. In this review, we highlight recent strategies for alignment and patterning of ordered SMOSN and their corresponding device applications.

Keywords: small-molecule organic seminconductor micro/nanocrystals, alignment and patterning, device applications

Xiujuan Zhang, Jiansheng Jie, Wei Deng, Qixun Shang, Jincheng Wang, Hui Wang, Xianfeng Chen, Liming Huang, and Xiaohong Zhang**

Alignment and Patterning of Ordered Small-molecule Organic Semiconductor Micro/nanocrystals for Device Applications